

The Interplay of Spectral Efficiency, User Density, and Energy in Random Access Protocols with Retransmissions

Derya Malak

Abstract

The fifth-generation of wireless communication networks is required to support a range of use cases such as enhanced mobile broadband (eMBB), ultra-reliable, low-latency communications (URLLC), massive machine-type communications (mMTCs), with heterogeneous data rate, delay, and power requirements. The 4G LTE air interface uses extra overhead to enable scheduled access, which is not justified for small payload sizes. We employ a random access communication model with retransmissions for multiple users with small payloads at the low spectral efficiency regime. The radio resources are split non-orthogonally in the time and frequency dimensions. Retransmissions are combined via Hybrid Automatic Repeat reQuest (HARQ) methods, namely Chase Combining and Incremental Redundancy with a finite buffer size constraint C_{buf} . We determine the best scaling for the spectral efficiency (SE) versus signal-to-noise ratio (SNR) per bit and for the user density versus SNR per bit, for the sum-optimal regime and when the interference is treated as noise, using a Shannon capacity approximation. Numerical results show that the scaling results are applicable over a range of η , T , C_{buf} , J , at low received SNR values. The proposed analytical framework provides insights for resource allocation in general random access systems and specific 5G use cases for massive URLLC uplink access.

Index Terms

Multiple access, NOMA, HARQ, Chase combining, Incremental redundancy, spectral efficiency, SNR per bit, user density, matched filter decoding, maximum ratio combining, and HARQ receiver buffer.

D. Malak is with the Communication Systems Department, EURECOM, Biot Sophia Antipolis, 06904 FRANCE (email: derya.malak@eurecom.fr).

The material in this paper will be presented in part at the 20th Int. Symp. Modeling and Optim. in Mobile, Ad Hoc, and Wireless Netw. (WiOpt 2022), Turin, Italy [1].

I. INTRODUCTION

The fifth-generation (5G) communication networks will support a wide range of use cases beyond high data rate applications, including Ultra-reliable, low-latency communication (URLLC) settings with small payload sizes transmitted by a large number of users with stringent power requirements. 4G LTE cannot effectively handle the heterogeneity because it ensures interference-free transmission via scheduled access and is designed to support fewer devices with large payloads. On the other hand, the overhead of scheduled access in 4G LTE is not desirable in URLLC applications.

Motivated by the challenges in scheduled access, we consider a wireless multiple access communication channel (MAC) model where a set of users sends their fixed payloads (in bits) given a preallocation of uplink resources. A given set of shared spectral resources of bandwidth ω Hertz (Hz) is partitioned into B frequency bins which are shared by the users in a non-orthogonal manner via non-orthogonal multiple access (NOMA), and the time of duration τ second (sec) which is uniformly divided into T time slots, i.e., transmit opportunities. For a given blocklength n , the total dimension in a given channel use is $m = n/T$. We consider different forms of Hybrid Automatic Repeat reQuest (HARQ): (i) HARQ with Chase Combining of NOMA transmissions, CC-NOMA, (ii) HARQ with chase combining of OMA transmissions, CC-OMA, and (iii) HARQ with Incremental Redundancy, IR-OMA. The general challenge is to design a random access protocol to maximize the scaling of the density of users versus the SNR per bit.

Via the proposed retransmission-based random access scheme, we aim to address the following central questions for 5G wireless networks and beyond:

- The spectral efficiency (SE, which denotes the total number of data bits per total real number of degrees of freedom, rdof) versus signal-to-noise ratio (SNR) per bit (or equivalently E_b/N_0) tradeoff for different HARQ schemes with retransmissions via Chase combining or Incremental redundancy. What are the gains in the sum-optimal technique versus the gains of the approach based on treating interference as noise (TIN)?
- How sensitive is the scaling of the SE versus E_b/N_0 to the number of retransmissions, T , different SNR, ρ , regimes, different uplink load J regimes, where we keep the total power is fixed?
- The blocklength, n , versus the number of retransmissions, T . We assume that the time is slotted and each slot $t = 1, \dots, T$ accommodates the transmission of a block of m symbols. How does signal-to-interference-plus-noise ratio (SINR) change with $n = mT$, where m denotes the blocklength per retransmission?

- The impact of a finite HARQ buffer size on the throughput of HARQ. The size of the buffer available at the receiver to store previously received packets impacts the throughput of retransmission-based schemes. The buffer capacity is mC_{buf} , where C_{buf} is the buffer size normalized with the packet lengths. How does C_{buf} affect the scaling performances?
- NOMA-based signalling and the effect of user signature (random and non-orthogonal) correlations, denoted by the non-orthogonality factor¹ η , on the scaling of the user density J/n (users/r dof) versus E_b/N_0 given a number of users, J . How should we design η for the conventional matched filter receiver (MFR) for single-user detection (SUD) for decoding of random signatures? How does the scaling behavior of J/n change as function of T ?

We next review the connections to the state-of-the-art and summarize the bottlenecks.

A. Related Work

Random access models and scaling of throughput. Random-access protocols have been pioneered with the emergence of ALOHA [3] and slotted or reservation-based ALOHA [4], [5] schemes, which later yielded the development of carrier sense multiple access (CSMA). However, these contention-based schemes do not have desirable throughput and delay performances and do not guarantee a deterministic load. Recently, different uplink schemes have been proposed to accommodate massive access [6]. In general, the resource being shared is on a time-frequency grid, and each transmission costs one time-frequency slot, and the signal strengths provide a new dimension at the receiver. An information theoretic analysis for massive user connectivity has been conducted in [7] through a dof perspective to characterize the throughput via incorporating the device identification, where the users are assigned orthogonal time-frequency resource blocks. Other models include sparse code multiple access (SCMA) for grant-free multiple access [8], multi-user detectors (MUDs) that improve performance of random-CDMA [9], [10] for spread spectrum systems (in different bases), e.g., orthogonal multiple access (OMA) coded OFDM, or CDMA with random non-orthogonal spreading, and generally NOMA [11]. Other works have focused on the capacity of Gaussian multiple access channels (MAC) [12], many-access channels with user identification [13], quasi-static fading MAC [14], Gaussian MAC with noiseless feedback [15], and with noisy feedback [16]. Finite-blocklength achievability bounds for the Gaussian MAC and random access channel (RAC) under average-error and maximal-power

¹The non-orthogonality metric, denoted by η , can be made sufficiently small for large blocklengths. For our model with blocklength $m = \frac{n}{T}$ per transmission, $\eta \approx \frac{1}{\sqrt{m}}$ [2].

constraints have been devised in [17], with single-bit feedback from the decoder to instruct the encoder when to stop transmitting.

Interference management and resource sharing. Different interference management techniques have been studied under different spectral efficiency models. To accommodate massive random access, interference cancellation [18], collision resolution [6], load control [19], and interference cancellation given a target outage rate [20] have been proposed.

From the perspective of fundamental limits, the best achievable rate region for two user Gaussian interference channel is given by Han-Kobayashi [21]. Interference alignment is a good technique when there are multiple interferers for specific channel parameters [22], [23], [24], [25]. However, the capacity region in the presence of multiple interferers is unknown because ideal interference cancellation is not practical for a large number of users. In [26], we characterized the scaling of throughput (user density) with deadline under outage constraints for a suboptimal but more practical random access system where the time and frequency domains are slotted. The receiver uses conventional SUD, which decodes a desired user's data by treating other users' interfering signals as noise, subject to an SINR-based outage constraint. However, the main limitation is the fixed per-user power, which causes a linear scaling between the received SNR and the number of users.

Critical performance metrics. Using different power levels to reduce E_b/N_0 has been considered in [27]. Random linear coding with approximate message passing (AMP) decoding for many-user Gaussian MAC has been studied in [28], where the authors derive the asymptotic error rate achieved for a given user density, user payload (in bits), and user energy (and energy per bit versus user density tradeoff). Cognitive radio and NOMA have been blended to maximize the achievable rate of the secondary user without deteriorating the outage performance of primary user [29]. Dynamic power allocation and decoding order at the base station for two-user uplink cooperative NOMA-based cellular networks has been studied in [30], where the authors demonstrated the superior performance over traditional two-user uplink NOMA (without cooperation).

HARQ models and generation of coding sequences. HARQ is a combination of Automatic Repeat reQuest (ARQ) and forward error correction (FEC) [31]. In particular, there are three models known as HARQ with Selective Repeat, HARQ with CC, and HARQ with IR [32], [33], [34]. This one is a salient variant of HARQ that captures puncturing via parity bits, e.g., puncturing with Turbo codes [35], and effects of different HARQ buffer sizes [36]. In general, it is well known that successive refinement of information can provide an optimal description from a rate-distortion perspective [37], [38], and incremental refinements and multiple descriptions with feedback have been explored [39].

Coding sequences have been devised for massive access, including Walsh sequences and decorrelated sequences [40], or almost affinely disjoint subspaces [41], where it is possible to characterize the Hamming weight distribution of pseudorandom sequences [42], and Khachatrian-Martirosian construction to enable $K > n$ users signal in n dimensions simultaneously, where $K \approx \frac{1}{2}n \log_2 n$ is the optimal scaling [2, Slides 57-59]. Furthermore, it has been shown that when the inputs are constrained to ± 1 , it is possible to have $K \gg n$. Zadoff-Chu sequences provide low complexity and constant-amplitude output signals, and have been widely used in 3GPP LTE air interface, including the control and traffic channels [43]. Sequence design for grant-free MAC has been contemplated in [44], where the authors devised uniquely-decodable multi-amplitude sequences. However, this approach induces a high E_b/N_0 , which is not desirable in a practical massive access scenario for users with small payloads.

B. Overview, Contributions and Organization

The goal of this paper is to analyze a retransmission-based general random access framework that unifies the properties of NOMA-based transmissions with HARQ-based protocols that rely on CC and IR to provide insights on uplink resource allocation strategies for future 5G wireless communication networks. In Section II, we describe the system model for random access and detail the key performance metrics, SE (bits/r dof), the SNR per bit (E_b/N_0), and user density (users/r dof) for a given blocklength, total received power constraint, and a total number of retransmissions. We delineate the retransmission-based random access schemes in Section III and analyze their SE and the SNR per bit for the sum-optimal and TIN cases. More specifically, we consider several retransmission-based models where the receiver jointly decodes transmissions via (i) the classical transmission scheme with no retransmissions, and the retransmission-based schemes using different combining techniques, namely (ii) CC-NOMA, (iii) CC-OMA, and (iv) IR-OMA. In Section IV, we numerically evaluate the scaling results, namely the SE versus SNR per bit and user density versus SNR per bit tradeoffs, and show the behavior with an increasing number of transmissions T , received SNR ρ , the HARQ buffer size C_{buf} , the non-orthogonality factor η , and the total number of users J .

The key design insights for the proposed random access framework are as follows:

- **The low ρ regime is relevant.** Our framework exploits the conventional MFR for SUD and is suitable at low SNRs ρ . We show that the user density of NOMA-based models scales significantly better at low ρ versus high ρ . The interference cannot be exploited at high ρ , which degrades the performance of TIN-based models. Furthermore, the minimum SNR per bit to achieve a non-zero user density grows with ρ .

- **The SE of the sum-optimal strategy improves with NOMA.** Compared to OMA-based transmissions, CC-NOMA has a better SE vs E_b/N_0 performance. The performance of IR-OMA approaches the performance of the classical model as C_{buf} at the receiver increases.
- **The SE of the TIN strategy is optimal at low ρ .** Provided that C_{buf} is sufficiently large, TIN is good at low SE. If not, a higher T is required. The scaling results are sensitive to η for CC-NOMA, and a codebook with smaller η can significantly improve the SE of TIN.
- **User density is sensitive to retransmissions.** For the sum-optimal model, although the performances of CC-OMA, IR-OMA, and the classical techniques degrade with increasing T , CC-NOMA does not sacrifice the number of users per rdof as much. We also note that a higher number of users J , when the per user power is kept fixed, results in a lowered received SNR ρ per user, which improves the SE for the sum-optimal CC-NOMA model, yet for the TIN-based model, the SINR drops due to the higher effective interference, which degrades the SE for a given SNR per bit. For TIN, CC-OMA and CC-NOMA perform well at low ρ values and CC-OMA can effectively combine retransmissions even at higher values of ρ . However, the SNR per bit requirement of CC-NOMA is very sensitive to ρ , which deteriorates the performance at high ρ values. The SE of the classical model and IR-OMA do not scale as well as CC-OMA because the former models cannot compensate for the interference at high ρ , hence cannot leverage the retransmissions attempts.
- **User density scales up with SNR per bit.** The user density J/n can superlinearly scale with E_b/N_0 (where the scaling does not necessarily degrade with T in the case of CC-NOMA versus the other models that rely on OMA) in the infinite blocklength (IBL) regime, which gives an upper bound to the actual user density scaling. As n increases, these upper bounds become tighter. Both for the sum-optimal and the TIN-based models, the scaling of the user density versus SNR per bit does not improve with ρ due to the increase in the SNR per bit.

Our insights could be applied to 5G wireless system design with delay and resource-constrained communications, which is critical in use cases such as URLLC or mMTC. Nevertheless, the scaling results in our framework provide an upper bound on the achievable SE and the user density because of the following additional assumptions: ideal negative acknowledgment with no error or delay, the IBL regime capacity-achieving encoding, perfect power control, perfect synchronization among users, and decoding via a suboptimal receiver, through matched filtering and SUDs, versus MUD, which could strictly improve performance of random-CDMA [2, slide 146]. Our analysis does not incorporate the fading, e.g., exponentially distributed interference power (i.e., Rayleigh fading) or path loss, and the

capacity for the FBL channel model. Therefore, a more general framework that allows studying these key points will be considered as a future work, as detailed in Section V.

II. SYSTEM MODEL

We consider a wireless random access communication model where a collection of users transmits over shared radio resources to a common receiver. The goal of each user is to transmit its payload of fixed size (L bits) within a latency constraint (blocklength n). A user is granted T retransmission attempts, i.e., time slots, to communicate its payload. The users use non-orthogonal signatures to transmit their payloads, as shown in Fig. 1-(a). The signatures are kept identical at each attempt.

Frame structure. Each frame has a total bandwidth of ω Hertz (Hz) and the time of duration τ second (sec), which is partitioned into B frequency bins of equal width, and T time slots, i.e., transmit opportunities, of equal duration. We refer to a given frequency bin and time slot as a time-frequency slot (TFS). For the proposed frame structure, the number of resources or real degrees of freedom (rdof) in a frame is $N = \omega\tau$. The total number of rdof N is evenly split into T retransmissions. The time-frequency resources in a frame are shared by a collection of users in a non-orthogonal manner. Each user attempts to transmit its payload of fixed size L bits over shared resources. Note that given ω , τ , m , and T , the number of symbols in a TFS is $\omega\tau/(BT)$. Under the orthogonal division of the resources, the coding rate is $LBT/(\omega\tau)$ bits per transmitted symbol.

User (source) model. Given T (re)transmission attempts, the total blocklength n per user is split uniformly across T attempts to accommodate the retransmission of a packet. Hence, the blocklength per transmission at each time slot is $m = n/T$. Let J_t be the number of users at slot $t \in \{1, \dots, T\}$, \mathcal{J}_t be the set of users at slot t such that $J = \sum_{t=1}^T J_t$, and \mathcal{J} be the set of all users in the frame.

Let $\mathbf{U}_j = (U_{j1}, U_{j2}, \dots, U_{jK})$ be the K dimensional source vector corresponding to user $j \in \mathcal{J}$. In the case of no feedback, we model each retransmission from user j with a blocklength m by $\mathbf{X}_{tj} = (X_{tj1}, X_{tj2}, \dots, X_{tjm})$, where we assume that the transmitted signal from user j is given by $\mathbf{X}_{tj} = \phi_{tji}(\mathbf{U}_j) = a_{tj}\mathbf{S}_j$, where $a_{tj} \in \mathbb{C}$ denotes the complex amplitude of the transmitted symbol of user j at slot t , and \mathbf{S}_j denotes its signature (spreading sequence), respectively. Let $\phi_{tji} : \mathcal{U}_j^K \rightarrow \mathcal{X}_j$ for $i = 1, \dots, m$ be the encoder function of $j \in \mathcal{J}$ for retransmission attempt $t \in \{1, \dots, T\}$.

User signatures. The number of rdof N in a frame can be thought of as the total length of the signature sequences of the active users over B frequency bins. Each user has the same signature across all time-frequency resources. The TFSs are shared in a non-orthogonal manner, where each waveform at a given time slot is a sum of non-orthogonal signatures, which is indicated in Fig. 1-(a). We assume

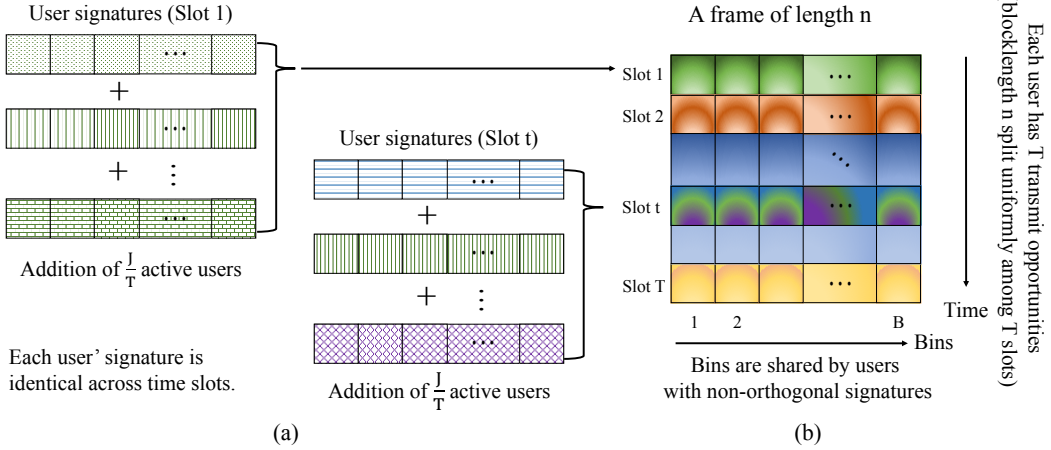


Fig. 1: (a) Non-orthogonal user signatures at time slots 1 and t . Each user uses the same signature across all time-frequency resources. The second user in slot 1 is repeated in slot t (same signature). (b) The frame structure where time is partitioned into T transmit opportunities, and the time-frequency resources are shared in a non-orthogonal manner by the users.

that \mathbf{S}_j are unitary, $\|\mathbf{S}_j\| = 1$, and $|\langle \mathbf{S}_j, \mathbf{S}_{j'} \rangle| = \eta$ for any $\{(j, j') \in \mathcal{J}_t : j \neq j'\}$. The maximum value of J_t to ensure that all $j \in \mathcal{J}_t$ is decoded with zero-error is given by the Khachatrian-Martirosian² construction [2] allows $J_t > m$ users. Under this setup, when \mathbf{S}_j 's are random and m is large $\eta \approx \frac{1}{\sqrt{m}}$ with high probability. We illustrate the frame structure with overlapping NOMA traffic in Fig. 1-(b).

Received signal and conventional matched filter decoding. We denote the received signal vector during transmission $t \in \{1, \dots, T\}$ by $\mathbf{Y}_t = (Y_{t1}, Y_{t2}, \dots, Y_{tm})$. We also let $\mathbf{Y}_t^i = (Y_{t1}, Y_{t2}, \dots, Y_{ti})$. In the case with feedback, the channel input from user j at time $i \in \{1, \dots, m\}$ for retransmission attempt $t \in \{1, \dots, T\}$, the encoder function of $j \in \mathcal{J}$ is $\phi_{tji} : \mathcal{U}_j^K \times \mathcal{Y}^{i-1} \rightarrow \mathcal{X}_j$ for $i = 1, \dots, m$ where $X_{tji} = \phi_{tji}(\mathbf{U}_j, \mathbf{Y}_t^{i-1})$. We leave the setting with feedback as future work. The channel is additive such that the received signal vector during transmission t is

$$\mathbf{Y}_t = \mathbf{X}_{tj} + \sum_{j' \in \mathcal{S}_{t,-j}} \mathbf{X}_{tj'} + \mathbf{Z}_t = a_{tj} \mathbf{S}_j + \sum_{j' \in \mathcal{S}_{t,-j}} a_{tj'} \mathbf{S}_{j'} + \mathbf{Z}_t, \quad (1)$$

where $\mathcal{S}_{t,-j}$ is the collection of the interferers of $j \in \mathcal{J}_t$ in the same time slot t , i.e., $\mathcal{S}_{t,-j} = \{j' \in \mathcal{J}_t : j' \neq j\}$, and $\mathbf{Z}_t \sim \mathcal{CN}(0, \sigma_t^2 I_m)$ is a complex Gaussian random variable.

We consider the *conventional matched filter receiver* (MFR) for decoding, which performs approximately optimal when the target SINR is low. In this case, the effective bandwidth required by the

²In the case of a binary adder channel (BAC) to signal in m dimensions simultaneously with zero-error, it holds that $J_t \approx \frac{1}{2} m \log_2 m$ (optimal). For 2 users, the maximal sum rate in the FBL regime satisfies $\frac{3}{2} + c\sqrt{\frac{1}{n}} \log n \geq R_{sum}(n, \epsilon) \geq \frac{3}{2} - \sqrt{\frac{1}{4n}} Q^{-1}(\epsilon) + O(\log n)$.

conventional approach is small versus the linear decorrelator receiver, which is desired as it allows many users per dof, where the other users' signals are treated as additive white Gaussian noise (AWGN) [10]. On the other hand, when the target SINR is high, both the linear minimum mean-square error (MMSE) and the linear decorrelator receiver decorrelate a user from the rest, yielding no more than one dof per interferer [10]. In the case that $\{\mathbf{S}_j\}_{j \in \mathcal{J}}$ are known to the receiver, an MMSE-based receiver provides a better signal-to-interference ratio (SIR) per user via exploiting the structure of the interference [10]. The maximum number of supported users for the MFR in the asymptotic regime is derived in [10] as a function of a target SIR, SIR^* , and the received power, P , under power control. It is given as $\frac{1}{\text{SIR}^*} - \frac{\sigma^2}{P}$, which increases in P , and is equal to $\frac{1}{\text{SIR}^*}$ when P tends to infinity.

Maximum ratio combining. We assume that the receiver's HARQ buffer size equals the number of coded symbols per coded packet, where the retransmitted packets are summed up with previously received erroneous packets via maximum ratio combining (MRC) of retransmissions prior to decoding.

The common receiver has the decoder function $\Phi_T : \mathcal{Y}^n \rightarrow \{\mathcal{U}_j^K\}_j$ that combines T retransmissions to decode the individual source vectors $\{\mathbf{U}_j\}_j$ from the received signal vector \mathbf{Y}_t during transmission $t \in \{1, \dots, T\}$ from the transmitted signals $\{\mathbf{X}_{tj}\}_{j \in \mathcal{J}_t}$. Using (1), the MRC of T transmissions results in the following combined signal:

$$\mathbf{Y} = \mathbf{U}_j + \sum_{t=1}^T a_{tj}^* \sum_{j' \in \mathcal{S}_{t,-j}} a_{tj'} \mathbf{S}_{j'} + \mathbf{Z}, \quad (2)$$

where $\mathbf{Y} = \sum_{t=1}^T a_{tj}^* \mathbf{Y}_t$, and $\mathbf{U}_j = \sum_{t=1}^T |a_{tj}|^2 \mathbf{S}_j$, and $\mathbf{Z} = \sum_{t=1}^T a_{tj}^* \mathbf{Z}_t$ are m dimensional vectors.

Per user received SNR. The noise power each user sees is assumed to be additive and constant with value σ_t^2 , $t \in \{1, \dots, T\}$ per dimension, i.e., $\mathbb{E}[\langle \mathbf{Z}_t, \mathbf{Z}_t \rangle] = m\sigma_t^2$, where $m\sigma_t^2$ is the total noise power across the number of frequency bins, which is B . The energy constraint for each source $j \in \mathcal{J}$ at any given $t \in \{1, \dots, T\}$ is

$$\frac{1}{T} \mathbb{E}[\mathbf{U}_j^T \mathbf{U}_j] = \sum_{i=1}^m \mathbb{E}[X_{tji}^2] = \mathbb{E}[\mathbf{X}_{tj}^T \mathbf{X}_{tj}] = m\sigma_t^2 \rho_{tj} \leq \frac{KE_j}{T}, \quad (3)$$

i.e., the total power of channel input linearly scales with the message size K , where the received power of user $j \in \mathcal{J}$ normalized with respect to K is E_j . We assume that $\mathbb{E}[X_{tji}] = 0$ and X_{tji} 's across $j \in \mathcal{J}$ are not independent such that $\mathbb{E}[\mathbf{X}_{tj}^T \mathbf{X}_{tj'}] \leq \frac{KE_{jj'}}{T}$ for $\{(j, j') : j \neq j'\}$.

Assuming that $\mathbb{E}[X_{tji}^2]$ does not change with $i \in \{1, \dots, m\}$, and $\sigma_t^2 = \sigma^2$, from (3) we have

$$\rho_{tj} = \frac{\mathbb{E}[\mathbf{X}_{tj}^T \mathbf{X}_{tj}]}{m\sigma^2} = \frac{1}{m\sigma^2} \sum_{i=1}^m \mathbb{E}[X_{tji}^2] = \frac{\mathbb{E}[X_{tji}^2]}{\sigma^2} = \frac{|a_{tj}|^2}{m\sigma^2}, \quad j \in \mathcal{J}.$$

We further assume that ρ_{tj} are identical and denoted by ρ . Given a constant received power of $\sigma^2\rho$, the received SNR equals ρ . The relation between ρ and σ^2 is given as $\rho = \frac{1}{\sigma^2}\mathbb{E}[\mathbf{X}_{tj}^T \mathbf{X}_{tj}]$. We note that the total power spent by all users is

$$P_{tot} = \frac{JTm\sigma^2\rho}{n} = J\sigma^2\rho, \quad (4)$$

or equivalently, the total energy spent for a given blocklength n is nP_{tot} .

The overall problem is to determine some key performance metrics and their joint behavior. More specifically, we will explore the behavior of the spectral efficiency, the SNR per bit, and the user density, which we describe in the sequel.

a) Spectral efficiency: The spectral efficiency, SE, is the maximum number of bits per channel use (bits/s/Hz):

$$\text{SE} = \frac{\text{Total number of data bits}}{\text{rdof}}, \quad (5)$$

where rdof represents the total number of real dof, n .

Definition 1. (Achievable channel coding rate [45].) A rate R is achievable with complete feedback for a discrete memoryless channel (DMC) $p(y|x)$ if for any $\epsilon > 0$, there exists for sufficiently large n an (n, M) code with complete feedback such that

$$\frac{1}{n} \log M > R - \epsilon.$$

Assume that a user attempts to transmit a payload of fixed size L bits over the channel. Hence, the relation between the required codebook size M and L is $L = \log M$. Hence, the blocklength n should be chosen sufficiently large so that the achievable transmit rate, $\frac{L}{n}$, satisfies:

$$\frac{L}{n} \leq C = \frac{1}{2} \log_2(1 + \text{SINR}) \quad \text{bit/rdof}, \quad n \leq N, \quad (6)$$

where C is Shannon's channel capacity, and SINR represents the signal-to-interference-plus-noise ratio, for an AWGN channel where interference is treated as noise (TIN). Shannon's channel capacity is achievable at an arbitrarily low error rate when coding is performed in the IBL regime, i.e., using a

code block of $n \rightarrow \infty$. However, since N is finite, the ratio L/N is always finite. Hence, given L , the IBL scheme gives an upper bound on the achievable rate, and a lower bound on n .

When the blocklength n is finite, i.e., in the finite blocklength (FBL) regime, the maximal rate achievable is approximated by [46]

$$R(n, \epsilon) = \frac{1}{n} \log M(n, \epsilon) \approx C - \sqrt{\frac{V}{2n}} Q^{-1}(\epsilon), \quad (7)$$

where $M(n, \epsilon)$ is the maximal code size achievable with a given blocklength n and average error probability ϵ , and $Q(x) = \frac{1}{\sqrt{2\pi}} \int_x^\infty e^{-u^2/2} du$ is the tail probability of the standard normal distribution where Q^{-1} is the inverse Q -function. Furthermore, in (7), V is the channel dispersion given by $V = 1 - \frac{1}{(1+\text{SINR})^2}$, and for the AWGN channel model by TIN, C is Shannon's channel capacity, which satisfies (6). We note that at low ρ , the value of SINR is small and the channel dispersion in the FBL regime becomes negligible, yielding from (7) that the IBL approximation is good in the TIN regime. For more details on the FBL regime, we refer the reader to [46].

b) SNR per bit: The SNR per bit, E_b/N_0 , represents the ratio of the energy-per-bit to the noise power spectral density, which is a normalized SNR measure:

$$\frac{E_b}{N_0} = \frac{\text{Total energy spent}}{2 \times \text{Total number of bits}}, \quad (8)$$

which is dimensionless, and usually expressed in decibels (dB).

c) User density: User density (users/r dof), J/n , represents the total number of users per dof that can transmit within the same frame (of which J_t/n denotes the density of users that can simultaneously transmit in slot t), for a given total blocklength n for the given frame duration. From (5), (6), and (8) it is clear that the achievable user density for a given n is affected by the SE vs SNR per bit tradeoffs of the retransmission-based protocols for uplink access, which we detail in Section III.

III. COMBINING NOMA-BASED RETRANSMISSIONS IN UPLINK

We focus on the scaling behaviors of the SE, the SNR per bit, and the user density for the retransmission-based random access schemes. The senders must contend not only with the receiver noise but also with interference from each other. To that end, we next analyze the behavior of the SE and SNR per bit performances of the HARQ-based schemes for the sum-optimal regime and via TIN.

A. The Classical Transmission Scheme with No Multiplexing of Retransmissions

We commence with the classical interference-based model with no multiplexing across different time slots. The time resources are split uniformly across T slots. There are $J_t = J/T$ users per slot sharing the frame resources. The SE of the classical sum-optimal transmission approach is given as

$$R_{\text{sum}}^{\text{Clas.}} = \frac{1}{2} \log_2 \left(1 + \rho \frac{J}{T} \right) \quad \text{bit/rdof} . \quad (9)$$

The SNR per bit of the classical sum-optimal transmission model is equal to

$$\frac{E_b}{N_0} = \frac{J\sigma^2\rho n}{m \log_2 \left(1 + \rho \frac{J}{T} \right)} = \frac{J\sigma^2\rho T}{\log_2 \left(1 + \rho \frac{J}{T} \right)} . \quad (10)$$

From (9) and (10), for the classical sum rate optimal approach when $T = 1$, the measures SE and P_{tot} satisfy the relation $\frac{(2^{2\text{SE}}-1)\sigma^2}{2\text{SE}} = \frac{P_{\text{tot}}}{\log_2(1+P_{\text{tot}}/\sigma^2)}$, where SE is given in (9), and P_{tot} is given in (4).

The SE of the classical model via TIN is expressed as

$$R_{\text{TIN}}^{\text{Clas.}} = \frac{J}{2T} \log_2 \left(1 + \frac{\rho}{\rho(\frac{J}{T} - 1) + 1} \right) \quad \text{bit/rdof} . \quad (11)$$

Similarly, the SNR per bit for the classical TIN transmission model is given as

$$\frac{E_b}{N_0} = \frac{T\sigma^2\rho}{\log_2 \left(1 + \frac{\rho}{\rho(\frac{J}{T} - 1) + 1} \right)} . \quad (12)$$

We note from L'Hôpital's rule under fixed total power P_{tot} and $T = 1$ that $\lim_{\rho \rightarrow 0} \frac{E_b}{N_0} = \log 2 \cdot P_{\text{tot}}$. From (11) and (12), for the classical TIN transmission approach when $T = 1$, the measures SE, P_{tot} , and J satisfy the relation $\frac{(2^{\frac{2\text{SE}}{J}} - 1)}{2\text{SE} \left[1 - (J-1)(2^{\frac{2\text{SE}}{J}} - 1) \right]} = \frac{\rho}{\log_2 \left(1 + \frac{\rho}{P_{\text{tot}}/\sigma^2 - \rho + 1} \right)}$, where SE is given in (11).

In general, transmissions are exposed to different channel conditions, more specifically the fading (e.g., exponentially distributed interference power, i.e., Rayleigh fading) or path loss. The channel gains $|H_{jt}|^2$, as function of $t = 1, \dots, T$ and $j \in \mathcal{J}$ can be incorporated into the system model, assuming that $|H_{jt}|^2$ has unit power and is independent across the slots with a known cumulative distribution function (CDF), $F_{|H|^2}$. Incorporating the channel gains, we can express the SE of the classical sum-optimal model as

$$R_{\text{sum}}^{\text{Clas.}} = \frac{1}{2T} \sum_{t=1}^T \log_2 \left(1 + \rho \sum_{j \in \mathcal{J}_t} |H_{jt}|^2 \right) \quad \text{bit/rdof} .$$

Similarly, the SNR per bit for the classical sum-optimal model is

$$\frac{E_b}{N_0} = \frac{J\sigma^2\rho n}{\frac{m}{T} \sum_{t=1}^T \log_2 \left(1 + \rho \sum_{j \in \mathcal{J}_t} |H_{jt}|^2 \right)} .$$

A more comprehensive SINR model with the channel gains will be considered as a future direction.

In the case of no retransmissions, TIN is essentially optimal for low SE [2]. However, for strategies that combine the retransmissions, TIN may not be optimal even at low SE. We will later demonstrate in Sections III-B, III-C, and III-D, and via numerical simulations in Section IV that sum-optimal capacity models could be more energy efficient via combining of retransmissions versus TIN.

B. Chase Combining with NOMA-based Retransmissions

In CC-HARQ, each transmission contains the same data and parity bits. The receiver's HARQ buffer size for CC-HARQ equals the number of coded symbols per coded packet, where the retransmitted packets are summed up with previously received erroneous packets via MRC of retransmissions prior to decoding. In Fig. 2 (top), we sketch CC-HARQ, where the retransmitted packets are to be summed at the receiver prior to decoder. We next derive the SE for the Chase combining of NOMA-based retransmissions (CC-NOMA) for the sum rate optimal model.

Proposition 1. Chase combining of non-orthogonal transmissions. *The SE of CC-NOMA for the sum rate optimal model is expressed by the following upper bound:*

$$R_{\text{sum}}^{\text{CC,NOMA}} = \frac{1}{2} \log_2 \left(1 + \rho T \left[1 + \eta^2 \left(\frac{1}{T} \sum_{t=1}^T J_t - 1 \right)^2 \right] \right) \quad \text{bit/rdoF} . \quad (13)$$

Proof. See Appendix A. □

Using (8), the SNR per bit for CC-NOMA for the sum rate optimal model is given as

$$\frac{E_b}{N_0} = \frac{J\sigma^2\rho}{\log_2 \left(1 + \rho T \left[1 + \eta^2 \left(\frac{J}{T} - 1 \right)^2 \right] \right)} . \quad (14)$$

We next provide a lower bound on E_b/N_0 , which is followed by a limit as $\rho \rightarrow 0$.

Corollary 1. A lower bound on E_b/N_0 . *The SNR per bit for CC-NOMA for the sum rate optimal model is lower bounded as*

$$\frac{E_b}{N_0} \geq -1.59\text{dB} + 10 \log_{10} J\sigma^2 - 10 \log_{10} T \left[1 + \eta^2 \left(\frac{J}{T} - 1 \right)^2 \right] . \quad (15)$$

Proof. From (13) and (14), we have

$$\begin{aligned} \frac{E_b}{N_0} &= J\sigma^2 \cdot \frac{1}{T \left[1 + \eta^2 \left(\frac{J}{T} - 1 \right)^2 \right]} \cdot \frac{(2^{2SE} - 1)}{2SE} \\ &\geq -1.59dB + 10 \log_{10} J\sigma^2 - 10 \log_{10} T \left[1 + \eta^2 \left(\frac{J}{T} - 1 \right)^2 \right], \end{aligned}$$

where the inequality is due to $\frac{2^{2SE}-1}{2SE} \geq -1.59dB$ as $SE \rightarrow 0$. \square

Corollary 2. Sensitivity of the E_b/N_0 limit vs J for CC-NOMA under the sum rate optimal model. Given a finite P_{tot} , in the limit as $\rho \rightarrow 0$, the SNR per bit of the sum rate optimal approach is

$$\lim_{\rho \rightarrow 0} \frac{E_b}{N_0} = \log 2 \cdot P_{tot}. \quad (16)$$

Proof. Taking the limit of (14) as $\rho \rightarrow 0$, or as $J \rightarrow \infty$ for a given finite P_{tot} , we obtain

$$\begin{aligned} \lim_{J \rightarrow \infty} \frac{E_b}{N_0} &= \lim_{J \rightarrow \infty} \log 2 \cdot \frac{\sigma^2 \rho \left(1 + \rho T \left[1 + \eta^2 \left(\frac{J}{T} - 1 \right)^2 \right] \right)}{\rho T \eta^2 2 \left(\frac{J}{T} - 1 \right)^{\frac{1}{T}}} \\ &= \lim_{J \rightarrow \infty} \log 2 \cdot \sigma^2 \rho T \left(\frac{J}{T} - 1 \right) = \log 2 \cdot P_{tot}, \end{aligned}$$

where the first step follows from L'Hôpital's rule, and the last step from $P_{tot} = J\sigma^2\rho$. \square

Cor. 2 implies that when $P_{tot} = J\sigma^2\rho$ scales by a factor of A , then the SE curve for the sum-optimal capacity model moves to the left by $10 \log_{10} A$ dB, as demonstrated in Section IV (see e.g., Fig. 4).

The SE for CC-NOMA with TIN is

$$R_{\text{TIN}}^{\text{CC,NOMA}} = \frac{J}{2T} \log_2 \left(1 + \frac{\rho T^2}{T + \rho \eta^2 (J - T)^2} \right) \quad \text{bit/rdof}. \quad (17)$$

As $\rho \rightarrow \infty$, $SE \rightarrow \frac{1}{2 \log_2 T} \log \left(1 + \frac{T^2}{\eta^2 (J - T)^2} \right)$. Hence, $\rho \leq \frac{1}{2 \log_2 T} \log \left(1 + \frac{T^2}{\eta^2 (J - T)^2} \right)$.

The SNR per bit of CC-NOMA under TIN is given as:

$$\frac{E_b}{N_0} = \frac{J\sigma^2 \rho n}{n \frac{J}{T} \log_2 \left(1 + \frac{\rho T^2}{T + \rho \eta^2 (J - T)^2} \right)}. \quad (18)$$

We next provide a lower bound on E_b/N_0 , which is followed by a limit as $\rho \rightarrow 0$.

Corollary 3. A lower bound on E_b/N_0 . The SNR per bit of CC-NOMA under TIN satisfies

$$\frac{E_b}{N_0} \geq -1.59dB + 10 \log_{10} \sigma^2. \quad (19)$$

Proof. From (17) and (18), we have

$$\begin{aligned} \frac{E_b}{N_0} &= \frac{J\sigma^2\rho n}{n\frac{J}{T}\log_2\left(1 + \frac{\rho T^2}{T + \rho\eta^2(J-T)^2}\right)} \\ &= J\sigma^2 \cdot \frac{\frac{1}{T}(2^{\frac{2T}{J}SE} - 1)}{1 - \eta^2\left(\frac{J}{T} - 1\right)^2(2^{\frac{2T}{J}SE} - 1)} \cdot \frac{1}{2SE} \geq -1.59dB + 10\log_{10}\sigma^2, \end{aligned} \quad (20)$$

where the last step follows from using $\frac{2^{2SE}-1}{2SE} \geq 10\log_{10}(\log 2) = -1.59dB$ as $SE \rightarrow 0$. \square

Corollary 4. Sensitivity of the SNR per bit limit vs J for CC-NOMA under TIN. *For a given finite J , the SNR per bit via TIN approaches the following lower bound in the limit as $\rho \rightarrow 0$:*

$$\lim_{\rho \rightarrow 0} \frac{E_b}{N_0} = \log 2 \cdot \sigma^2, \quad (21)$$

which implies that the SNR per bit limit for TIN is not sensitive to J .

Proof. Taking the limit of (18) as $\rho \rightarrow 0$, and incorporating the relation $P_{tot} = J\sigma^2\rho$, we obtain

$$\begin{aligned} \lim_{\rho \rightarrow 0} \frac{E_b}{N_0} &= \lim_{\rho \rightarrow 0} \frac{J\sigma^2\rho n}{n\frac{J}{T}\log_2\left(1 + \frac{\rho T^2}{T + \rho\eta^2(J-T)^2}\right)} \\ &= \lim_{\rho \rightarrow 0} \log 2 \cdot \frac{T\sigma^2\rho}{\frac{\rho T^2}{T + \rho\eta^2\left(\frac{P_{tot}}{\sigma^2\rho} - T\right)^2}} = \lim_{\rho \rightarrow 0} \log 2 \cdot \frac{\sigma^2}{T} \left(T + \rho\eta^2\left(\frac{P_{tot}}{\sigma^2\rho} - T\right)^2\right). \end{aligned} \quad (22)$$

For a given finite J , in the limit as $\rho \rightarrow 0$, E_b/N_0 goes to $\log 2 \cdot \sigma^2$, where P_{tot} goes to 0. \square

From (22), under a given finite P_{tot} , the scaling of ρ is inversely proportional to the scaling of J , and when P_{tot} is held fixed, the E_b/N_0 limit scales with ρ^{-1} .

C. Chase Combining with OMA-based Retransmissions

In this model, the retransmissions of each user are combined to enhance its received SNR. This scheme is a simplified version of CC-NOMA where the users have orthogonal messages, namely OMA with chase combining or CC-OMA, which was introduced in [26]. We next provide its SE.

Proposition 2. Chase combining of orthogonal transmissions. *The SE for CC-OMA with the sum-optimal capacity model is given as*

$$R_{\text{sum}}^{\text{CC,OMA}} = \frac{1}{2} \log_2 \left(1 + \rho T \left[1 + \frac{1}{T} \left(\frac{J}{T} - 1 \right) \right] \right) \quad \text{bit/rdoF}. \quad (23)$$

Proof. See Appendix B. □

The SNR per bit of $R_{\text{sum}}^{\text{CC,OMA}}$ is given as

$$\frac{E_b}{N_0} = \frac{J\sigma^2\rho n}{n \log_2 \left(1 + \rho T \left[1 + \frac{1}{T} \left(\frac{J}{T} - 1 \right) \right] \right)}. \quad (24)$$

The SE of CC-OMA with TIN is given as

$$R_{\text{TIN}}^{\text{CC,OMA}} = \frac{J}{2T} \log_2 \left(1 + \frac{\rho T}{1 + \rho \left(\frac{J}{T} - 1 \right)} \right) \quad \text{bit/rdof}. \quad (25)$$

In the limit as $J \rightarrow \infty$, it holds that $R_{\text{TIN}}^{\text{CC,OMA}} \leq \frac{T}{2 \log 2}$. The subsequent result follows using the definition (8) for SNR per bit and the SE given in (25).

Corollary 5. *The SNR per bit of $R_{\text{TIN}}^{\text{CC,OMA}}$ satisfies the lower bound given as*

$$\frac{E_b}{N_0} \geq -1.59\text{dB} + 10 \log_{10} \sigma^2. \quad (26)$$

Proof. The SNR per bit of $R_{\text{TIN}}^{\text{CC,OMA}}$ is given as

$$\begin{aligned} \frac{E_b}{N_0} &= \frac{J\sigma^2\rho n}{n \frac{J}{T} \log_2 \left(1 + \frac{\rho T}{1 + \rho \left(\frac{J}{T} - 1 \right)} \right)} \\ &= J\sigma^2 \cdot \frac{\frac{1}{T} (2^{\text{SE} \frac{2T}{J}} - 1)}{1 - \frac{1}{T} \left(\frac{J}{T} - 1 \right) (2^{\text{SE} \frac{2T}{J}} - 1)} \cdot \frac{1}{2\text{SE}} \geq -1.59\text{dB} + 10 \log_{10} \sigma^2, \end{aligned} \quad (27)$$

where the second equality follows from using (25) which yields $\rho = \frac{(2^{\text{SE} \frac{2T}{J}} - 1)}{T - \left(\frac{J}{T} - 1 \right) (2^{\text{SE} \frac{2T}{J}} - 1)}$, and the last step follows from the same intuition as in (15) and (18). □

D. Incremental Redundancy with OMA-based Retransmissions

In this section, we consider an incremental redundancy model with OMA (IR-OMA). From Sections III-B and III-C, due to the finite HARQ buffer size, the throughput of CC-NOMA is determined by the addition of all active users' signals at any given time slot. Hence, a finite HARQ buffer has an impact on the throughput of HARQ. Unlike CC-NOMA, in IR-OMA every retransmission contains different information than the previous one. Furthermore, different from CC, where the buffer size is the same as the number of packets per transmission, in IR-OMA, which is also known as HARQ Type III, the buffer size is equal to the number of coded bits of the total transmitted coded packets, where each retransmitted packet is self-decodable.

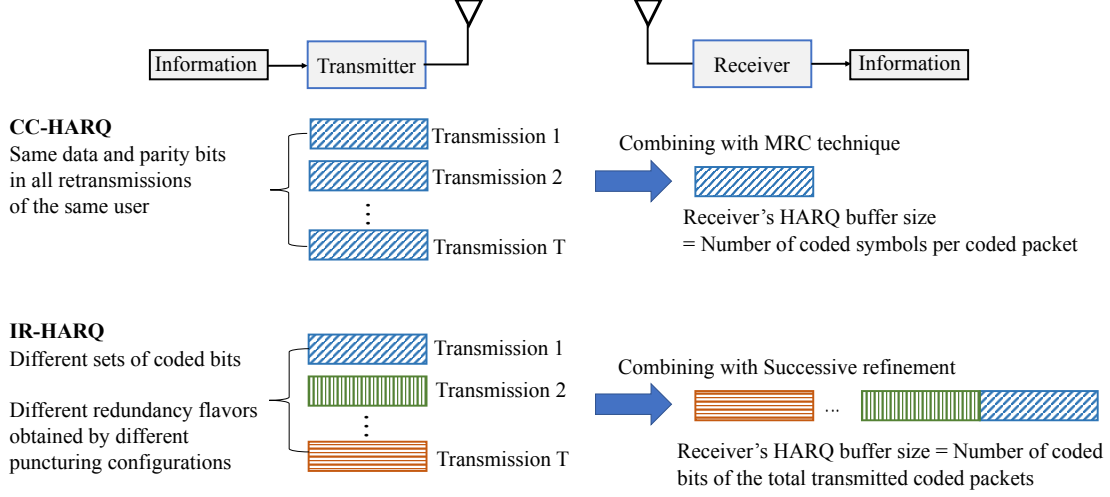


Fig. 2: (Top) CC-HARQ, where the retransmissions contain the same data and parity bits, which are summed at the receiver prior to decoding. (Bottom) IR-HARQ, where each retransmission provides some additional bits, and is self-decodable.

In IR-HARQ, multiple different sets of code bits are generated for the same information bits used in a packet. Each set of coded bits is transmitted under different channel conditions. These sets consist of different redundant flavors obtained by different puncturing configurations. In Fig. 2 (bottom), we sketch IR-HARQ, where each retransmitted packet provides some additional information bits, and is self decodable, i.e., it provides successive refinement [37] by iteratively improving the rate-distortion tradeoff as more information is transmitted.

Expected quantization distortion. Using the refinement-based approach in [37], the average quantization distortion is characterized as the mean squared error distortion between the quantized signal $\hat{\mathbf{Y}}_{t,T}$ and the received signal \mathbf{Y}_t . The quantized m dimensional signals are given by $\hat{\mathbf{Y}}_{t,T} = \mathbf{Y}_t + \mathbf{Q}_{t,T}$. The quantization noise satisfies $\mathbf{Q}_{t,T} \sim \mathcal{CN}(0, \frac{2\sigma_q^2(t,T)}{m} I_m)$, where $\sigma_q^2(t, T)$ represents the total quantization noise power per rdof (the quantization distortion per frequency bin is $\sigma_q^2(t, T)/B$) for IR-OMA at slot t given a total number of T retransmissions, where attempt t is unsuccessful if $1 \leq t < T$ and the retransmission is successful at attempt T . From (1), \mathbf{Y}_t has a dimension $m = n/T$.

Proposition 3. The sum rate of IR-OMA. *The SE for IR-OMA with the sum-optimal model equals*

$$R_{\text{sum}}^{\text{IR,OMA}} = \frac{B}{2} \log_2 \left(1 + \frac{\rho J \sigma^2 / B}{\sigma^2} \right) + \sum_{t=1}^{T-1} \frac{B}{2} \log_2 \left(1 + \frac{\rho J \sigma^2 / B}{\sigma^2 + \sigma_q^2(t, T-1) / B} \right) \quad \text{bit/rdof}/(T \text{ slots}), \quad (28)$$

where the quantization noise as function of C_{buf} is

$$\sigma_q^2(t, T) = \begin{cases} \frac{B(J\rho/B+1)\sigma^2}{2^{\frac{2C_{\text{buf}}}{TB}} - 1}, & t < T, \\ 0, & t = T. \end{cases} \quad (29)$$

Proof. See Appendix C. □

Note that in Prop. 3, $\log_2\left(1 + \frac{\rho J \sigma^2}{\sigma^2}\right) \leq \frac{B}{2} \log_2\left(1 + \frac{\rho J \sigma^2 / B}{\sigma^2}\right)$, which follows from employing $\sum_{i=1}^n \log(1 + x_i) \leq n \log\left(1 + \frac{1}{n} \sum_{i=1}^n x_i\right)$ with $x_1 = 1$ and $x_i = 0, i \neq 1$. We do not focus on optimizing the number of non-overlapping frequency bins B and dividing total transmit power, which is left as future work. Instead, in Section IV, we let $B = 1$ to provide lower bounds on the performance tradeoffs.

We next express the SNR per bit for IR-OMA for sum-optimal case.

Proposition 4. *The SNR per bit of IR-OMA for sum-optimal case is given as*

$$\frac{E_b}{N_0} = \frac{J\sigma^2\rho}{\frac{B}{T} \sum_{t=1}^T \log_2\left(1 + \frac{\rho J / B}{1 + \sigma_q^2(t, T-1) / (B\sigma^2)}\right)}, \quad (30)$$

where $\sigma_q^2(t, T-1)$ for $t \leq T-1$ can be derived from (29), and $\sigma_q^2(T, T-1) = 0$.

Proof. See Appendix D. □

As the buffer size $C_{\text{buf}} \rightarrow \infty$, $\frac{E_b}{N_0} \rightarrow \frac{J\sigma^2\rho}{\log_2(1+\rho J)}$. Similarly, for smaller C_{buf} , $\frac{E_b}{N_0} > \frac{J\sigma^2\rho}{\log_2(1+\rho J)}$. Hence, it is easy to note that as C_{buf} increases the IR-OMA sum SE matches the sum SE for the classical problem without combining transmissions (sum-optimal case). However, when C_{buf} is small the gap between the SE for the classical transmission model and the IR-OMA sum SE grows as T increases.

Proposition 5. The SE of TIN for IR-OMA. *The SE for IR-OMA with TIN is given as*

$$\begin{aligned} R_{\text{TIN}}^{\text{IR,OMA}} &= \frac{JB}{2T} \log_2\left(1 + \frac{\rho\sigma^2/B}{\rho\sigma^2/B(J/T-1) + \sigma^2}\right) \\ &+ \sum_{t=1}^{T-1} \frac{JB}{2T} \log_2\left(1 + \frac{\rho\sigma^2/B}{\rho\sigma^2/B(J/T-1) + \sigma^2 + \sigma_q^2(t, T-1)/B}\right) \quad \text{bit/rdof}/(T \text{ slots}), \end{aligned} \quad (31)$$

where the buffer size normalized with respect to the packet lengths, i.e., C_{buf} , more precisely the transmit rate, provided that $C_{\text{buf}} < \frac{BT}{2} \log_2\left(1 + \frac{\rho\sigma^2/B + \sigma^2}{(J/T-1)\rho\sigma^2/B}\right)$, satisfies:

$$\frac{C_{\text{buf}}}{T} = \frac{B}{2} \log_2\left(1 + \frac{\rho\sigma^2/B + \sigma^2}{(J/T-1)\rho\sigma^2/B + \sigma_q^2(t, T)/B}\right), \quad (32)$$

which implies that as $\sigma_q^2(t, T) \rightarrow 0$ for $C_{\text{buf}} \geq \frac{BT}{2} \log_2 \left(1 + \frac{\rho\sigma^2/B + \sigma^2}{(J/T-1)\rho\sigma^2/B} \right)$, where the size of C_{buf} could be tuned to the channel capacity (7) in the FBL regime. The expression (32) leads to the following relation between the quantization noise $\sigma_q(t, T)$ and the buffer size C_{buf} :

$$\sigma_q^2(t, T) = \frac{B(\rho/B + 1)\sigma^2}{2^{\frac{2C_{\text{buf}}}{TB}} - 1} - (J/T - 1)\rho\sigma^2. \quad (33)$$

We next express the SNR per bit for IR-OMA under TIN.

Proposition 6. *The SNR per bit of IR-OMA for TIN is given as*

$$\frac{E_b}{N_0} = \frac{T\sigma^2\rho}{\frac{B}{T} \sum_{t=1}^T \log_2 \left(1 + \frac{\rho/B}{\rho\zeta_t/B+1} \right)}, \quad (34)$$

where $\zeta_t = (J/T - J/(T-1) + 1/(2^{(2C_{\text{buf}})/(T-1)B} - 1)) + B/\rho \cdot 1/(2^{(2C_{\text{buf}})/(T-1)B} - 1)$ for $t < T$, i.e., ζ_t is fixed for $t < T$, and $\zeta_T = (J/T - 1)$ when $t = T$.

Proof. See Appendix E. □

We next provide a limit on E_b/N_0 as $C_{\text{buf}} \rightarrow \infty$, which is followed by a limit as $\rho \rightarrow 0$.

Corollary 6. *As $C_{\text{buf}} \rightarrow \infty$, the SNR per bit for IR-OMA with TIN approaches*

$$\lim_{C_{\text{buf}} \rightarrow \infty} \frac{E_b}{N_0} = \frac{T\sigma^2\rho}{\log_2 \left(1 + \frac{\rho}{\rho(J/T-1)+1} \right)}. \quad (35)$$

Proof. From Prop. 6, as $C_{\text{buf}} \rightarrow \infty$, $\zeta_t = (J/T - J/(T-1))$ for $t < T$, and $\zeta_T = (J/T - 1)$, and the SNR per bit for IR-OMA with TIN approaches

$$\lim_{C_{\text{buf}} \rightarrow \infty} \frac{E_b}{N_0} = \frac{T\sigma^2\rho}{\frac{1}{T} \sum_{t=1}^T \log_2 \left(1 + \frac{\rho}{\rho\zeta_t+1} \right)} \leq \frac{T\sigma^2\rho}{\log_2 \left(1 + \frac{\rho}{\rho(J/T-1)+1} \right)}, \quad (36)$$

where the inequality in the second step is indeed an equality because $\sigma_q^2(t, T) \rightarrow 0$ as $C_{\text{buf}} \rightarrow \infty$, where (32) no longer holds, and the desired bit-error-rate (BER) is met from (31). □

The limit in (35) is the SNR per bit for the classical TIN transmission model in (12). In general, as $\rho \rightarrow 0$, for large buffer sizes C_{buf} , the following result is immediate from Prop. 6.

Corollary 7. *As $\rho \rightarrow 0$, for large buffer sizes C_{buf} , it holds for IR-OMA under TIN that*

$$\lim_{\rho \rightarrow 0} \frac{E_b}{N_0} \approx \log 2 \cdot P_{\text{tot}}. \quad (37)$$

For smaller C_{buf} , the ratio $\frac{E_b}{N_0}$ is typically larger than the SNR per bit for the classical TIN case.

For the different HARQ models in hand, next in Section IV, we will study the SE versus E_b/N_0 and J/n versus E_b/N_0 tradeoffs by exploiting the joint behavior of SE, E_b/N_0 , and ρ .

IV. NUMERICAL EVALUATION OF SCALING RESULTS

In this section, we first study the SE (bits/r dof) versus the E_b/N_0 (dB) tradeoff (see Figs. 3 and 4) for the different HARQ-based retransmission combining models for the sum-optimal and the TIN schemes detailed in Section III, as function of T , η , C_{buf} , and J . Our numerical results (in Figs. 3 and 4) are for the IBL regime, providing upper bounds to the actual scaling behaviors for the SE models. We then focus on the scaling behavior of the user density J/n with respect to E_b/N_0 (dB) (see Figs. 5, 6, and 7) as function of T , η , C_{buf} , and ρ . For various regimes of interest, we indicate the set of chosen parameters of the sum-optimal and the TIN schemes in the legend on each plot.

Number of retransmissions T . Increasing T degrades the SE of the sum-optimal model (with CC-NOMA (13) and CC-OMA (23)). The SE for the TIN (with CC-NOMA and CC-OMA) improves. We note for IR-OMA that as T increases, unlike CC-NOMA and CC-OMA, each retransmission contains less information for successive refinement of the signal. In terms of the SE vs E_b/N_0 behavior, for $T > 1$, TIN CC-OMA is better than TIN IR-OMA and TIN classical. This trend is also obvious from relations (11), (17), (25), and (31). The gap between TIN CC-OMA and TIN IR-OMA grows in T .

Finite buffer size C_{buf} at the decoder. From the SNR per bit for the classical TIN model (12) and the SNR per bit for the IR-OMA in (37), the SNR per bit for the classical TIN and the IR-OMA models have a matching fundamental E_b/N_0 limit when C_{buf} is sufficiently large for $\rho = 0$ for any given T . As C_{buf} becomes smaller the SNR per bit of IR-OMA increases versus the classical model. For large C_{buf} , the sum-optimal classical scheme and the sum-optimal IR-OMA scheme are the same (similar for TIN) (Fig. 3 (Row I)). From the same figure, in terms of the SE performance, we also observe that the sum-optimal CC-OMA is worse than TIN CC-OMA at low SNR per bit regime (and better than TIN CC-OMA at high SNR per bits), and TIN CC-OMA has a higher SE than TIN IR-OMA and the gains increase in T (Fig. 3 (Rows I-II)). For small C_{buf} , the performance of IR-OMA degrades both for the sum-optimal and TIN scenarios, as explained in Section III-D (Fig. 3 (Row III)). For large C_{buf} , the SE for TIN IR-OMA is higher (Fig. 3-(Row I)). The SE curves for IR-OMA with TIN and sum-optimal strategies are very close for small C_{buf} (for any given T), and for large C_{buf} the IR-OMA with TIN is approximately the same as the classical TIN, and the performance of IR-OMA in sum-optimal case approaches that of the classical sum-optimal model.

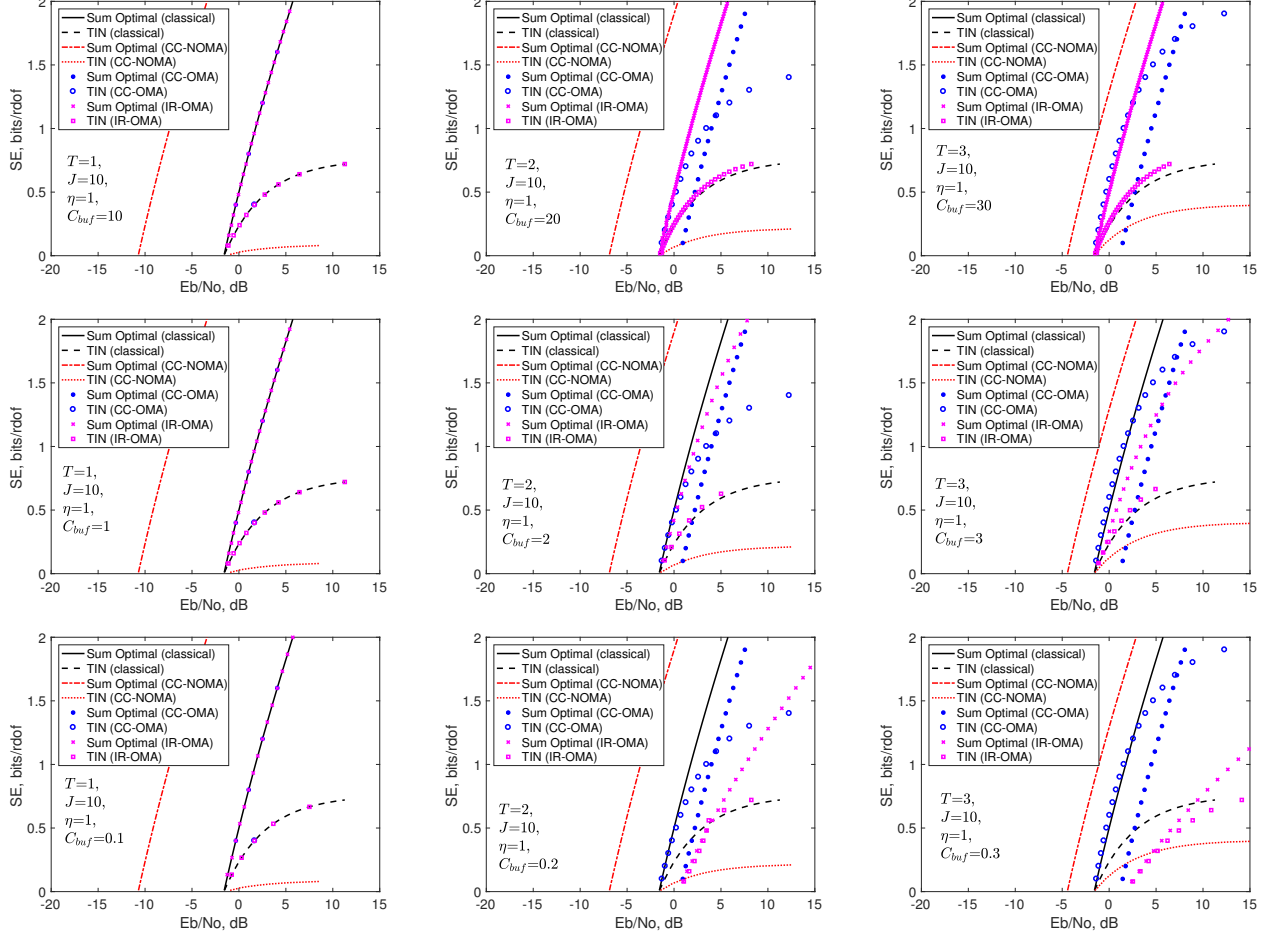


Fig. 3: Scaling of SE vs E_b/N_0 for varying T for $\eta = 1$ and $J = 10$. (Row I) large buffer size, $C_{\text{buf}} = 10T$. (Row II) moderate buffer size, $C_{\text{buf}} = T$. (Row III) small buffer size, $C_{\text{buf}} = 0.1T$.

Contrasting SE vs SNR per bit. We note for IR-OMA that as T increases, unlike the CC-NOMA and CC-OMA models, each retransmission contains less information to successively refine the signal to be decoded. For small C_{buf} , we expect the SE of IR-OMA to be a lower bound to these combining schemes. It can be observed that in terms of the SE vs SNR per bit tradeoff, for large C_{buf} , TIN IR-OMA can perform better than TIN CC-NOMA when interference is high (i.e., when $\eta = 1$ or J is high, which follows from the relation of (17) and (35)) and similar to classical TIN (follows from the equivalence of (11) to (31) as $\sigma_q^2(t, T-1) \rightarrow 0$ or equivalently $C_{\text{buf}} \rightarrow \infty$). When C_{buf} is small, i.e., under high quantization noise, the performance of TIN IR-OMA could be worse than TIN CC-NOMA and classical TIN for $T > 1$. For sum-optimal IR-OMA, for sufficiently large C_{buf} , the performance is in between sum-optimal CC-NOMA and sum-optimal CC-OMA, and interestingly sometimes better than CC-NOMA (when η is small from (13) and (28)). For large and moderate C_{buf} , the performance

of sum-optimal IR-OMA is in general better than CC-OMA and sometimes worse than CC-OMA when T is large and for moderate C_{buf} which requires a higher ρ (follows from the relations (23) and (28)). However, as C_{buf} decreases the performance of sum-optimal IR-OMA degrades. For the sum-optimal models, in the bandwidth-limited regime, i.e., when the SNR is high, the SE is less sensitive to the changes in ρ versus the changes in the power-limited region, i.e., when the SNR is low [47, Ch. 5].

Scaling of the SE of the sum-optimal scheme with J . Increasing J moves the SE for the sum-optimal model (with CC-NOMA) to the left (we refer the reader to the discussion right after (16)). For the TIN models (with CC-NOMA), the SE degrades with increasing J . This follows from (17) where the SE scales as $T/(J \log 2)$ as $J \rightarrow \infty$, and $J/T \log_2(1 + \rho T)$ as $J \rightarrow T$, i.e., no interference. Based on Cor. 4 (relation (21)) the SNR per bit E_b/N_0 of the TIN approach converges to a fixed constant as $\rho \rightarrow 0$ when J is kept fixed.

Non-orthogonality of transmissions measured via η . Based on the numerical experiments run for different values of measures η and J , as illustrated in Fig. 4, decreasing η in CC-NOMA reduces the effect of the interference, and improves the quality of the TIN models (with combining retransmissions). On the other hand, the SE for the sum-optimal model (with combining retransmissions) degrades.

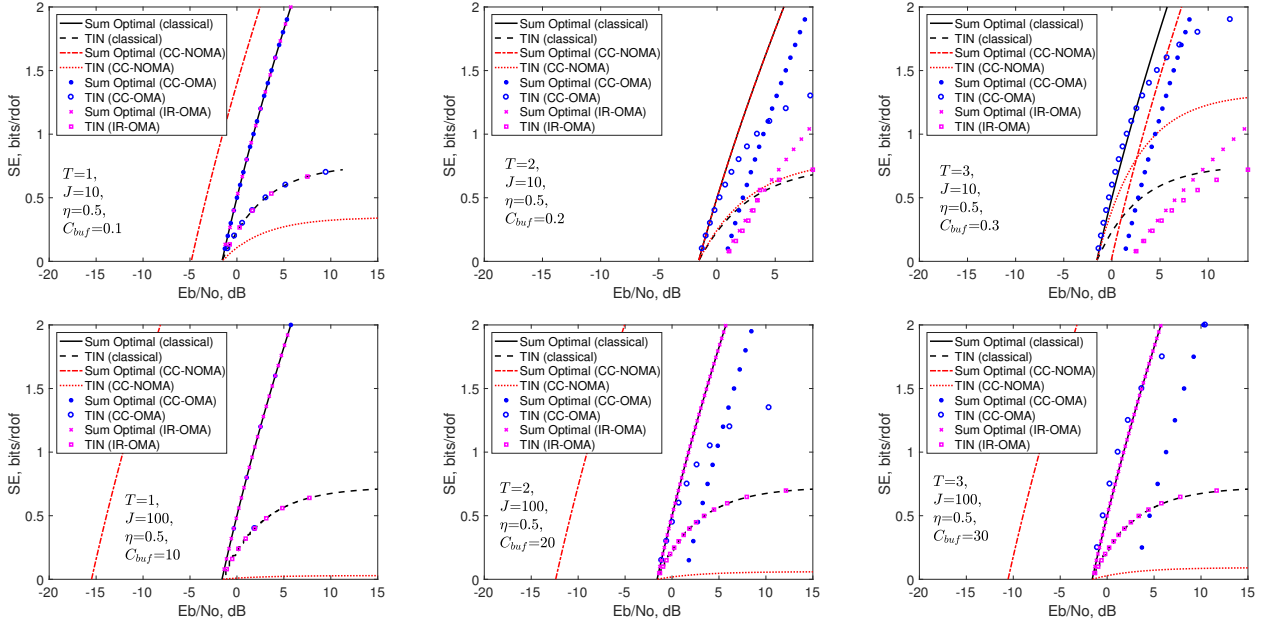


Fig. 4: Scaling of SE vs E_b/N_0 . (Row I) $\eta = 0.5$, $J = 10$, $C_{\text{buf}} = 0.1T$. (Row II) $\eta = 0.5$, $J = 100$, $C_{\text{buf}} = 10T$.

Scaling of user density J/n versus E_b/N_0 . We investigate this scaling behavior in Figs. 5, 6, and 7 as a function of ρ . A stricter average probability of error requirement at a decoder is equivalent to

a high ρ value, which yields a higher E_b/N_0 to achieve the same user density. Note also that as T increases, the blocklength per transmission, i.e., $m = n/T$, decreases, and the supported user density drops. We also note that as the received SNR ρ increases, the user scalings of different models for the sum-optimal strategy become similar under high C_{buf} . This is because the growth of E_b/N_0 is not much sensitive to ρ at low ρ and the approximate growth rate for the sum-optimal models is $\frac{\rho}{\log_2 \rho}$ for high ρ , which causes a significant drop in J/n . Furthermore, with the conventional MFR, which is effective at low SE, the optimal SE performance of the sum-rate optimal model cannot be accurately captured when ρ is high [10]. However, we might not observe this behavior for the TIN models under high C_{buf} (see last two rows of Fig. 7). For CC-NOMA from (18) E_b/N_0 roughly grows with $\eta^2(J-T)^2/T$ at low ρ and the scaling is subquadratic at high ρ , for CC-OMA from (27) E_b/N_0 grows with J/T at low ρ and the scaling becomes sublinear at high ρ . For the classical TIN model from (12), and similarly for IR-OMA at high C_{buf} , E_b/N_0 grows linearly with J at low ρ , and the behavior of J/T is not much sensitive to E_b/N_0 (unless E_b/N_0 grows faster than ρ) at high ρ . From (10), (14), (24), and (30), when $T = 1$, the classical model, CC-OMA, and IR-OMA behave the same, and CC-NOMA (14) has a lower ratio E_b/N_0 than (10), (24), and (30) for a given J/n . This behavior can be observed from Fig. 5 (Row I). In Fig. 5 (Rows II-III), the classical approach, from (10), the effective J/n for a given E_b/N_0 decays as a function of T . Similarly, for (14), (24), and (30). However, the scaling of these 3 is less sensitive vs the classical model (indicating their robustness). Note that from the most to least sensitive the ordering is classical, CC-OMA, IR-OMA, and CC-NOMA.

While retransmissions are inevitable in HARQ-based protocols, retransmission-based access schemes in general degrade the SE vs E_b/N_0 performance and similarly for J/n vs E_b/N_0 . For the sum-optimal model, in terms of the sensitivity of the J/n versus E_b/N_0 tradeoff with respect to increasing T , we have the ordering as the CC-NOMA model, the IR-OMA model, the CC-OMA model, and the classical model from the less sensitive (best) to the most sensitive (worst). For the TIN-based model, the CC-NOMA and the CC-OMA models improve the user density by increasing T , and the IR-OMA and the classical models are not robust to retransmissions. We also note that our numerical results for the sum-optimal SE models in Figs. 5 and 6 and the TIN models in Fig. 7 are for IBLs (i.e., providing upper bounds to the actual scaling behaviors). While the scaling performance improves with T , increasing T causes diminishing returns in gains. According to [12], the scalings for the FBL are linear instead of being exponential (subject to BER constraints). However, we note that unlike the setting in [12], where the total power P_{tot} is kept constant, we have a per user power constraint such that $P_{\text{tot}} = J\sigma^2\rho$, which scales linearly with J under fixed ρ .

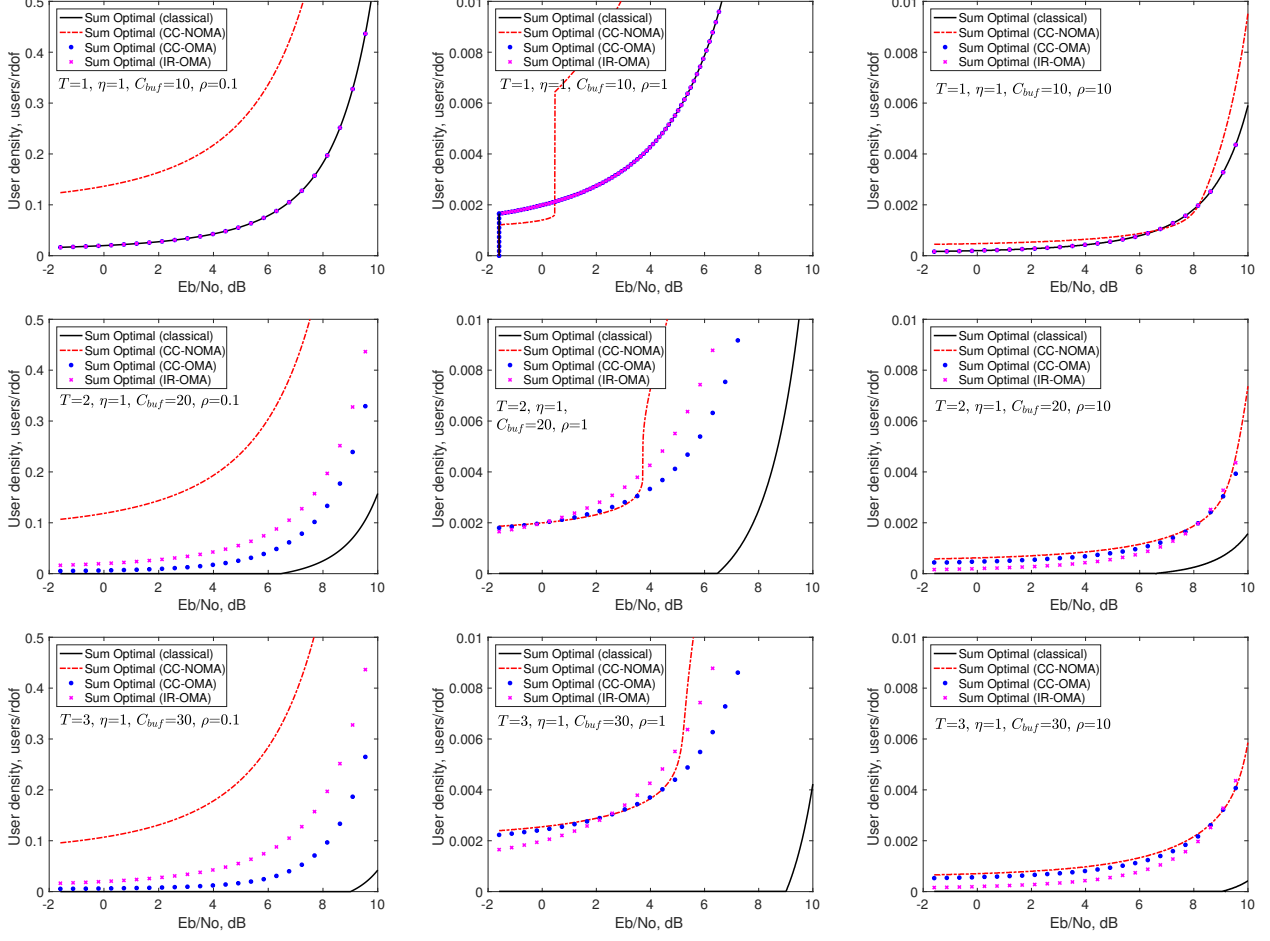


Fig. 5: (Sum-optimal) Scaling of J/n vs. E_b/N_0 for varying ρ and $C_{\text{buf}} = 10T$. (Rows I-III) $T = 1$, $T = 2$, and $T = 3$.

From Fig. 7, we observe that the different models we considered in this paper perform the best at low spectral efficiency. In other words, increasing ρ decreases the user density scaling performance for IR-OMA, CC-NOMA, and CC-OMA. To compensate for the loss of CC-NOMA, even though better coding signatures (lower η) can be incorporated, this model still requires a higher minimum SNR per bit versus the other models with a higher sensitivity to ρ . As T increases it is possible to achieve a higher number of users per rdof, and similarly, a better scaling for IR-OMA via increasing C_{buf} . At high C_{buf} (or high $\rho = 10$), IR-OMA yields a better performance over CC-OMA where CC-OMA scales better due to the combining of transmissions as given by the SNR per bit in the first step of (27) than IR-OMA with an SNR per bit in (34) (versus vice versa for lowered C_{buf} (or smaller $\rho \leq 1$)).

From Cor. 4, for CC-NOMA with the TIN model, the SNR per bit E_b/N_0 limit to ensure a nonzero user density increases with $\rho\eta^2$, and it is easy to notice from Fig. 7 (Row III) that this limit could

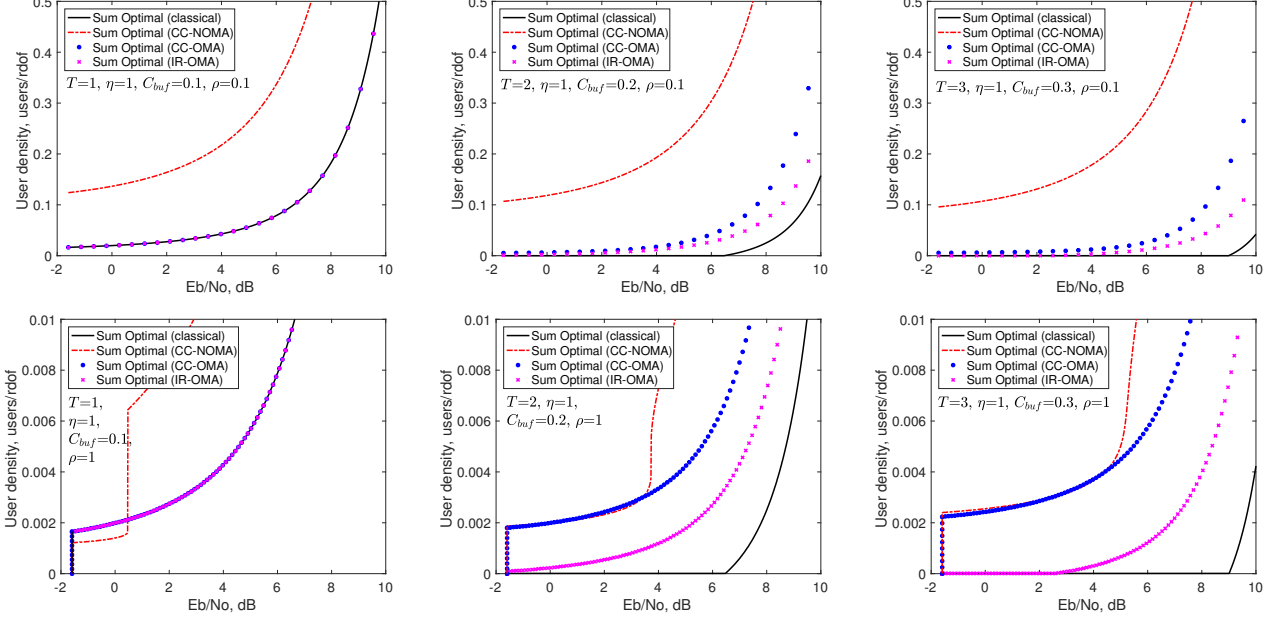


Fig. 6: (Sum-optimal) Scaling of J/n vs. E_b/N_0 and $C_{buf} = 0.1T$ for various T . (Row I) $\rho = 0.1$, (Row II) $\rho = 1$.

indeed be very large (i.e., > 10 dB). The conventional MFR approach is ideal for the low SINR regime, and with MFR, the characterization for the TIN-based might be suboptimal at high ρ [10].

V. CONCLUSIONS

In this paper, we considered several HARQ-based random access models for 5G wireless communication networks, where the receiver jointly decodes transmissions via (i) the classical transmission scheme with no retransmissions, and the retransmission-based schemes using different combining techniques, namely (ii) CC-NOMA, (iii) CC-OMA, and (iv) IR-OMA. We characterized the SE vs SNR per bit, and the user density vs SNR per bit tradeoffs, and demonstrated through numerical simulations that retransmissions can improve the scaling behaviors of SE and the user density. We further showed that the SE of the sum-optimal strategy improves with NOMA, and the SE via TIN is optimal at low SNR. In CC-NOMA, the sum user density is not affected much by retransmissions, and for IR-OMA the sensitivity decreases with C_{buf} .

Critical future directions include incorporating feedback and optimizing the number of retransmissions T and the number of frequency bins B . From a resource-allocation perspective, handling the issues of identification of user IDs, asynchrony, and traffic burstiness are of critical importance and left as future work. Another direction is the joint design of the physical and network layer aspects. It

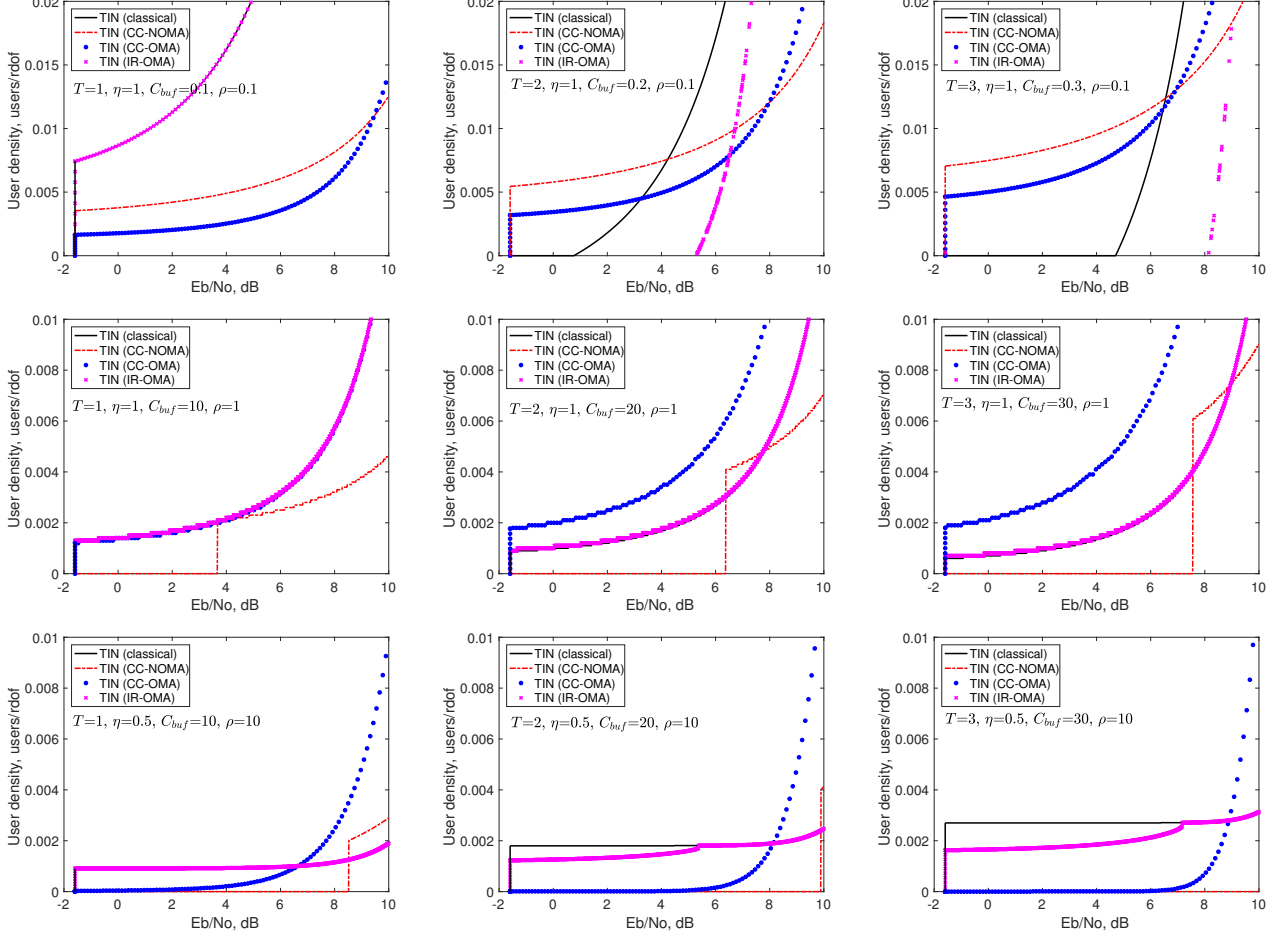


Fig. 7: (TIN) Scaling of J/n vs. E_b/N_0 for varying ρ and C_{buf} . (Row I) $\rho = .1$ and $C_{\text{buf}} = 0.1T$, (Row II) $\rho = 1$ and $C_{\text{buf}} = 10T$, (Row III) $\rho = 10$, $\eta = 0.5$ and $C_{\text{buf}} = 10T$.

is crucial to support heterogeneous traffic type requirements on one platform where distinct classes of users are under different SINR requirements. Power allocation for the cell edge versus cell center users could be different to mitigate the interference, and capacity model could be revisited under general power control mechanisms. Furthermore, the MMSE receiver is superior than the conventional MFR over a wide range of SIRs [10], which makes it more suitable under multiple traffic types.

The generalization of the classical capacity models to the FBL regime is of primary interest through incorporating channel gain, fading, or path loss, and outage capacity for IBL and FBL models, as well as techniques to achieve optimal performance for the SU and the MU settings. This will pave the way for understanding the 3-way tradeoff between SE , E_b/N_0 , and the payload L . In addition, the BER performance for the MU NOMA model depends on the modulation and coding scheme. The study of the asymptotic (IBL) or FBL probability of error (per user or for all users) achieved for a given user

density, user payload, and user energy, is left as future work.

APPENDIX

A. Proof of Prop. 1

We recall (1) and combining T transmissions results in

$$\sum_{t=1}^T a_{tj}^* \mathbf{Y}_t = \sum_{t=1}^T |a_{tj}|^2 \mathbf{S}_j + \sum_{t=1}^T a_{tj}^* \left(\sum_{j' \in \mathcal{S}_{t,-j}} a_{tj'} \mathbf{S}_{j'} + \mathbf{Z}_t \right).$$

Decoding via matched filter and SUDs, we obtain

$$\left\langle \mathbf{S}_j, \sum_{t=1}^T a_{tj}^* \mathbf{Y}_t \right\rangle = \sum_{t=1}^T |a_{tj}|^2 + \sum_{t=1}^T a_{tj}^* \sum_{j' \in \mathcal{S}_{t,-j}} a_{tj'} \langle \mathbf{S}_j, \mathbf{S}_{j'} \rangle + \sum_{t=1}^T a_{tj}^* \langle \mathbf{S}_j, \mathbf{Z}_t \rangle.$$

Total received signal power (for decoding j) is given as

$$P_S = \left(\sum_{t=1}^T |a_{tj}|^2 \right)^2. \quad (38)$$

Total noise (plus interference) power (by TIN) equals

$$\begin{aligned} & \left| \sum_{t=1}^T a_{tj}^* \sum_{j' \in \mathcal{S}_{t,-j}} a_{tj'} \langle \mathbf{S}_j, \mathbf{S}_{j'} \rangle + \sum_{t=1}^T a_{tj}^* \langle \mathbf{S}_j, \mathbf{Z}_t \rangle \right|^2 \\ &= \left| \sum_{t=1}^T a_{tj}^* \sum_{j' \in \mathcal{S}_{t,-j}} a_{tj'} \langle \mathbf{S}_j, \mathbf{S}_{j'} \rangle \right|^2 + \left(\sum_{t=1}^T a_{tj}^* \sum_{j' \in \mathcal{S}_{t,-j}} a_{tj'} \langle \mathbf{S}_j, \mathbf{S}_{j'} \rangle \right) a_{tj} \langle \mathbf{S}_j, \mathbf{Z}_t \rangle \\ &+ \left(\sum_{t=1}^T a_{tj} \sum_{j' \in \mathcal{S}_{t,-j}} a_{tj'}^* \langle \mathbf{S}_j, \mathbf{S}_{j'} \rangle^* \right) a_{tj}^* \langle \mathbf{S}_j, \mathbf{Z}_t \rangle^* + \sum_{t=1}^T |a_{tj}|^2 |\langle \mathbf{S}_j, \mathbf{Z}_t \rangle|^2 \\ &= \sum_{t=1}^T \sum_{t'=1}^T a_{tj} a_{t'j}^* \sum_{j' \in \mathcal{S}_{t,-j}} \sum_{k' \in \mathcal{S}_{t',-j}} a_{tj'}^* a_{t'k'} \langle \mathbf{S}_{j'}, \mathbf{S}_j \rangle \langle \mathbf{S}_j, \mathbf{S}_{k'} \rangle \\ &+ 2 \sum_{t=1}^T |a_{tj}|^2 \sum_{j' \in \mathcal{S}_{t,-j}} \text{Real}(a_{tj'} \langle \mathbf{S}_j, \mathbf{S}_{j'} \rangle \langle \mathbf{S}_j, \mathbf{Z}_t \rangle) + \sum_{t=1}^T |a_{tj}|^2 |\langle \mathbf{S}_j, \mathbf{Z}_t \rangle|^2. \end{aligned} \quad (39)$$

Computing the expected value of the total noise, we obtain

$$\begin{aligned} P_N &= \mathbb{E} \left[\left| \sum_{t=1}^T a_{tj}^* \sum_{j' \in \mathcal{S}_{t,-j}} a_{tj'} \langle \mathbf{S}_j, \mathbf{S}_{j'} \rangle + \sum_{t=1}^T a_{tj}^* \langle \mathbf{S}_j, \mathbf{Z}_t \rangle \right|^2 \right] \\ &= \sum_{t=1}^T \sum_{t'=1}^T a_{tj} a_{t'j}^* \sum_{j' \in \mathcal{S}_{t,-j}} \sum_{k' \in \mathcal{S}_{t',-j}} a_{tj'}^* a_{t'k'} \eta^2 + \sum_{t=1}^T |a_{tj}|^2 m \sigma_t^2 = \eta^2 \left| \sum_{t=1}^T \sum_{j' \in \mathcal{S}_{t,-j}} a_{tj} a_{tj'}^* \right|^2 + \sum_{t=1}^T |a_{tj}|^2 m \sigma_t^2. \end{aligned}$$

From (38) and (39), the total received power is $(Tm\sigma^2\rho)^2 + \eta^2(J-T)^2(m\sigma^2\rho)^2$. Rescaling this by the noise power, the SINR equals $T\rho\left[1 + \eta^2\left(\frac{J}{T} - 1\right)^2\right]$. Incorporating (3), the total capacity of the $J = \sum_{t=1}^T J_t$ user Gaussian MAC is given as

$$\sum_{t=1}^T \sum_{j \in \mathcal{J}_t} R_{tj} \leq \frac{1}{2} \log_2 \left(1 + \rho T \left[1 + \eta^2 \left(\frac{J}{T} - 1 \right)^2 \right] \right) \quad \text{bit/rdof} .$$

The SU decoder sees an effective SINR as a result of T transmissions given as

$$\text{SINR} = \left(\sum_{t=1}^T |a_{tj}|^2 \right)^2 / \left(\eta^2 \left| \sum_{t=1}^T \sum_{j' \in \mathcal{S}_{t,-j}} a_{tj} a_{tj'}^* \right|^2 + \sum_{t=1}^T |a_{tj}|^2 m \sigma_t^2 \right) \quad (40)$$

$$= \left(\sum_{t=1}^T \rho_{tj} m \sigma^2 \right)^2 / \left(\eta^2 \left| \sum_{t=1}^T \sum_{j' \in \mathcal{S}_{t,-j}} \sqrt{\rho_{tj} \rho_{tj'}} m \sigma^2 \right|^2 + \sum_{t=1}^T \rho_{tj} m \sigma^2 m \sigma^2 \right) \quad (41)$$

$$= \left(\sum_{t=1}^T \rho_{tj} \right)^2 / \left(\eta^2 \left| \sum_{t=1}^T \sum_{j' \in \mathcal{S}_{t,-j}} \sqrt{\rho_{tj} \rho_{tj'}} \right|^2 + \sum_{t=1}^T \rho_{tj} \right) \quad (42)$$

$$= \frac{(T\rho)^2}{\eta^2 \left(\sum_{t=1}^T (J_t - 1) \rho \right)^2 + T\rho} = \frac{\rho T^2}{T + \rho \eta^2 \left(\sum_{t=1}^T J_t - T \right)^2} \approx \frac{\rho T^2}{T + \frac{\rho}{m} \left(\sum_{t=1}^T J_t - T \right)^2} , \quad (43)$$

where (41) follows from $\sigma_t = \sigma$, (42) from dividing both the numerator and the denominator terms by $(m\sigma^2)^2$, and the last step in (43) from assuming that $\rho_{tj} = \rho$, and defining $\sum_{j' \in \mathcal{S}_{t,-j}} 1_{a_{tj'} \neq 0} = J_t - 1$.

B. Proof of Prop. 2

Combining T transmissions results in a noise power (by TIN):

$$P_N = \left(\sum_{t=1}^T a_{tj} \sum_{j' \in \mathcal{S}_{t,-j}} a_{tj'}^* \mathbf{S}_{j'}^* + \sum_{t=1}^T a_{tj} \mathbf{Z}_t^* \right) \left(\sum_{t=1}^T a_{tj}^* \sum_{j' \in \mathcal{S}_{t,-j}} a_{tj'} \mathbf{S}_{j'} + \sum_{t=1}^T a_{tj}^* \mathbf{Z}_t \right) \quad (44)$$

$$= \sum_{t=1}^T \sum_{t'=1}^T a_{tj} a_{t'j}^* \sum_{j' \in \mathcal{S}_{t,-j}} \sum_{k' \in \mathcal{S}_{t',-j}} a_{tj'}^* a_{t'k'} + \sum_{t=1}^T |a_{tj}|^2 \sigma_t^2 \quad (45)$$

$$= \sum_{t=1}^T \sum_{j' \in \mathcal{S}_{t,-j}} |a_{tj}|^2 |a_{tj'}|^2 + \sum_{t=1}^T \sum_{t' \neq t} \sum_{j' \in \mathcal{S}_{t,-j}} \sum_{k' \in \mathcal{S}_{t',-j}} (a_{tj}^* a_{t'j})^* (a_{tj'}^* a_{t'k'}) + \sum_{t=1}^T |a_{tj}|^2 \sigma_t^2 \quad (46)$$

$$= \sum_{t=1}^T \sum_{j' \in \mathcal{S}_{t,-j}} |a_{tj}|^2 |a_{tj'}|^2 + \sum_{t=1}^T |a_{tj}|^2 \sigma_t^2, \quad (47)$$

where (46) follows from assuming $\langle \mathbf{S}_j, \mathbf{S}_{j'} \rangle = 0$ for $j \neq j'$, and $a_{tj'}^* \cdot a_{tk'} = 0$ for $j' \neq k'$, and (47) follows from assuming $a_{tj}^* \cdot a_{t'j} = 0$ for $t' \neq t$ for all j and $\sigma_t^2 = \sigma^2$.

Letting $\rho_{tj} = \frac{\mathbb{E}[\mathbf{X}_{tj}^I \mathbf{X}_{tj}]}{\sigma^2} = \frac{|a_{tj}|^2}{\sigma^2} = \frac{1}{\sigma^2} \sum_{i=1}^m \mathbb{E}[X_{tji}^2]$, the effective SINR as a result of T transmissions is

$$\text{SINR} = \left(\sum_{t=1}^T \rho_{tj} \sigma^2 \right)^2 / \left(\sum_{t=1}^T \sum_{j' \in \mathcal{S}_{t,-j}} \rho_{tj} \sigma^2 \rho_{tj'} \sigma^2 + \sum_{t=1}^T \rho_{tj} \sigma^4 \right).$$

If ρ_{tj} are identical and equal to ρ , then defining $K_t = \sum_{j' \in \mathcal{S}_{t,-j}} 1_{a_{tj'} \neq 0} = J_t - 1$ the SU decoder sees an effective SINR, which is given as

$$\text{SINR} = \frac{\rho T^2}{\rho \sum_{t=1}^T K_t + T} = \frac{\rho T^2}{T + \rho \left(\sum_{t=1}^T J_t - T \right)}. \quad (48)$$

Reordering the terms in above equation, the SE for the sum-optimal capacity model is given by (23).

C. Proof of Prop. 3

Given the buffer size normalized with respect to the packet lengths, C_{buf} , the transmit rate is given by $\frac{mC_{\text{buf}}}{n} = \frac{C_{\text{buf}}}{T}$. We can relate the quantization noise $\sigma_q^2(t, T)$ to the number of allocated bits mC_{buf}/T via the rate-distortion theory [48]. Using (1) we infer, at transmission attempt t , $t < T$, it holds that

$$\frac{C_{\text{buf}}}{T} = I(\mathbf{Y}_t; \hat{\mathbf{Y}}_t) = \frac{B}{2} \log_2 \left(1 + \frac{J\rho\sigma^2/B + \sigma^2}{\sigma_q^2(t, T)/B} \right), \quad t < T, \quad (49)$$

which leads to the following relation between the quantization noise $\sigma_q(t, T)$ and the buffer size C_{buf} :

$$\sigma_q^2(t, T) = \frac{B(J\rho/B + 1)\sigma^2}{2^{\frac{2C_{\text{buf}}}{TB}} - 1}, \quad t < T, \quad (50)$$

where in (28) $\sigma_q^2(T, T) = 0$, i.e., at retransmission T , the received signal $\mathbf{Y}_T = \hat{\mathbf{Y}}_T$, i.e., the receiver recovers \mathbf{Y}_T . We also have the notational convention $\sigma_q^2(T, T-1) = 0$. Combining the retransmissions, each providing an addendum to the first transmission so that the signal as a result of T transmissions achieves the desired distortion, we obtain (28).

D. Proof of Prop. 4

The SNR per bit of IR-OMA for sum-optimal case is given as:

$$\begin{aligned}
\frac{E_b}{N_0} &= \frac{J\sigma^2\rho n}{2n\left(\frac{B}{2T}\log_2(1+\rho J/B) + \frac{(T-1)B}{2T}\log_2\left(1 + \frac{\rho J/B}{1+\sigma_q^2(t,T-1)/(B\sigma^2)}\right)\right)} \\
&= \frac{J\sigma^2\rho}{\frac{B}{T}\log_2(1+\rho J/B) + \frac{(T-1)B}{T}\log_2\left(1 + \frac{\rho J/B}{1+(J\rho/B+1)/(2^{\frac{2C_{\text{buf}}}{(T-1)B}}-1)}\right)} \\
&= \frac{J\sigma^2\rho}{\frac{B}{T}\log_2(1+\rho J/B) + \frac{(T-1)B}{T}\log_2\left(1 + \frac{\rho J(2^{\frac{2C_{\text{buf}}}{(T-1)B}-1}/B)}{J\rho/B+2^{\frac{2C_{\text{buf}}}{(T-1)B}}}\right)},
\end{aligned}$$

where the second line follows from (49) and (50) in Appendix C, yielding $\sigma_q^2(t, T-1) = \frac{B(J\rho/B+1)\sigma^2}{2^{\frac{2C_{\text{buf}}}{(T-1)B}-1}}$ for $t < T-1$, and using the notational convention $\sigma_q^2(T, T-1) = 0$. Note that as $C_{\text{buf}} \rightarrow \infty$, the E_b/N_0 result ($B=1$) is the same as the SNR per bit for the classical sum-optimal model in (10).

E. Proof of Prop. 6

Using (31), we can express the SNR per bit of IR-OMA for TIN as:

$$\begin{aligned}
\frac{E_b}{N_0} &= \frac{J\sigma^2\rho n}{2n\left(\frac{JB}{2T}\log_2\left(1 + \frac{\rho\sigma^2/B}{\rho\sigma^2/B(J/T-1)+\sigma^2}\right) + \frac{JB(T-1)}{2T}\log_2\left(1 + \frac{\rho\sigma^2/B}{\rho\sigma^2/B(J/T-1)+\sigma^2+\sigma_q^2(t,T-1)/B}\right)\right)/T} \\
&= \frac{T\sigma^2\rho}{\frac{B}{T}\log_2\left(1 + \frac{\rho/B}{\rho/B(J/T-1)+1}\right) + \frac{B(T-1)}{T}\log_2\left(1 + \frac{\rho/B}{\rho/B(J/T-1)+1+(\rho/B+1)/(2^{\frac{2C_{\text{buf}}}{(T-1)B}-1}-(J/(T-1)-1)\rho/B)}\right)} \\
&= \frac{T\sigma^2\rho}{\frac{B}{T}\log_2\left(1 + \frac{\rho/B}{\rho/B(J/T-1)+1}\right) + \frac{B(T-1)}{T}\log_2\left(1 + \frac{\rho/B}{1+\rho/B\left(J/T-J/(T-1)+1/(2^{\frac{2C_{\text{buf}}}{(T-1)B}-1})+1/(2^{\frac{2C_{\text{buf}}}{(T-1)B}-1})}\right)}\right)},
\end{aligned}$$

where the second step follows from incorporating (33), which states

$$\sigma_q^2(t, T) = \frac{B(\rho/B+1)\sigma^2}{2^{\frac{2C_{\text{buf}}}{TB}}-1} - (J/T-1)\rho\sigma^2.$$

Letting $\zeta_t = (J/T - J/(T-1) + 1/(2^{\frac{2C_{\text{buf}}}{(T-1)B}} - 1)) + B/\rho \cdot 1/(2^{\frac{2C_{\text{buf}}}{(T-1)B}} - 1)$ for $t < T$, i.e., ζ_t is fixed for $t < T$, and $\zeta_T = (J/T - 1)$ for $t = T$ yields the result of the proposition in (34).

REFERENCES

- [1] D. Malak, "Throughput and energy tradeoffs for retransmission-based random access protocols," in *Proc., IEEE WiOpt*, Sep. 2022.

- [2] Y. Polyanskiy, “Information theoretic perspective on massive multiple-access,” *Short Course (slides) Skoltech Inst. of Tech., Moscow, Russia*, Jul. 2018.
- [3] N. Abramson, “The ALOHA system: Another alternative for computer communications,” in *Proc., AFIPS*, Nov. 1970, pp. 281–285.
- [4] L. G. Roberts, “ALOHA packet system with and without slots and capture,” *ACM SIGCOMM Computer Commun. Review*, vol. 5, no. 2, pp. 28–42, Apr. 1975.
- [5] W. Crowther, R. Rettberg, D. Walden, S. Ornstein, and F. Heart, “A system for broadcast communication: Reservation-ALOHA,” in *Proc., 6th Hawaii Int. Conf. Syst. Sci.*, Jan. 1973, pp. 596–603.
- [6] G. C. Madueno, Č. Stefanović, and P. Popovski, “Efficient LTE access with collision resolution for massive M2M communications,” in *Proc., IEEE Globecom Wkshps*, Dec. 2014, pp. 1433–1438.
- [7] W. Yu, “On the fundamental limits of massive connectivity,” in *Proc., Inf. Theory and Apps. Wkshp (ITA)*, Feb. 2017, pp. 1–6.
- [8] A. Bayesteh, E. Yi, H. Nikopour, and H. Baligh, “Blind detection of SCMA for uplink grant-free multiple-access,” in *Proc., Int. Symp. Wireless Commun. Systems*, Aug. 2014, pp. 853–857.
- [9] S. Verdú and S. Shamai, “Spectral efficiency of CDMA with random spreading,” *IEEE Trans. Inf. Theory*, vol. 45, pp. 622–640, Mar. 1999.
- [10] D. N. C. Tse and S. V. Hanly, “Linear multiuser receivers: Effective interference, effective bandwidth and user capacity,” *IEEE Trans. Inf. Theory*, vol. 45, no. 2, pp. 641–657, Mar. 1999.
- [11] M. Vaezi, R. Schober, Z. Ding, and H. V. Poor, “Non-orthogonal multiple access: Common myths and critical questions,” *IEEE Wireless Commun.*, vol. 26, no. 5, pp. 174–180, Sep. 2019.
- [12] S. S. Kowshik and Y. Polyanskiy, “Fundamental limits of many-user MAC with finite payloads and fading,” *IEEE Trans. Inf. Theory*, vol. 67, no. 9, pp. 5853–5884, Jun. 2021.
- [13] X. Chen, T.-Y. Chen, and D. Guo, “Capacity of Gaussian many-access channels,” *IEEE Trans. Inf. Theory*, vol. 63, pp. 3516–39, Feb. 2017.
- [14] S. S. Kowshik and Y. Polyanskiy, “Quasi-static fading MAC with many users and finite payload,” in *Proc., IEEE ISIT*, Jul. 2019.
- [15] L. Ozarow, “The capacity of the white gaussian multiple access channel with feedback,” *IEEE Trans. Inf. Theory*, vol. 30, no. 4, pp. 623–629, Jul. 1984.
- [16] R. Tandon and S. Ulukus, “On the capacity region of the gaussian multiple access channel with noisy feedback,” in *Proc., IEEE Int. Conf. Commun.*, 2009, pp. 1–5.
- [17] R. C. Yavas, V. Kostina, and M. Effros, “Gaussian multiple and random access channels: Finite-blocklength analysis,” *IEEE Trans. Inf. Theory*, vol. 67, no. 11, pp. 6983–7009, Sep. 2021.
- [18] K. Dovelos, L. Toni, and P. Frossard, “Finite length performance of random MAC strategies,” in *Proc., IEEE ICC*, May 2017.
- [19] M. Koseoglu, “Pricing-based load control of M2M traffic for the LTE-A random access channel,” *IEEE Trans. Commun.*, vol. 65, no. 3, pp. 1353–1365, Dec. 2016.
- [20] H. S. Dhillon, H. C. Huang, H. Viswanathan, and R. A. Valenzuela, “Power-efficient system design for cellular-based machine-to-machine communications,” *IEEE Trans. Wireless Commun.*, vol. 12, no. 11, pp. 5740–5753, Oct. 2013.
- [21] T. Han and K. Kobayashi, “A new achievable rate region for the interference channel,” *IEEE Trans. Inf. Theory*, vol. 27, no. 1, pp. 49–60, Jan. 1981.
- [22] V. R. Cadambe, S. A. Jafar, and S. Shamai, “Interference alignment on the deterministic channel and application to fully connected gaussian interference networks,” *IEEE Trans. Inf. Theory*, vol. 55, no. 1, pp. 269–274, Dec. 2008.
- [23] C. Huang, V. R. Cadambe, and S. A. Jafar, “Interference alignment and the generalized degrees of freedom of the x channel,” *IEEE Trans. Inf. Theory*, vol. 58, no. 8, pp. 5130–5150, May 2012.
- [24] R. H. Etkin and E. Ordentlich, “The degrees-of-freedom of the k -user gaussian interference channel is discontinuous at rational channel coefficients,” *IEEE Trans. Inf. Theory*, vol. 55, no. 11, pp. 4932–4946, Oct. 2009.

- [25] V. R. Cadambe and S. A. Jafar, "Interference alignment and degrees of freedom of the k -user interference channel," *IEEE Trans. Inf. Theory*, vol. 54, no. 8, pp. 3425–3441, Jul. 2008.
- [26] D. Malak, H. Huang, and J. G. Andrews, "Throughput maximization for delay-sensitive random access communication," *IEEE Trans. Wireless Commun.*, vol. 18, no. 1, pp. 709–723, Dec. 2018.
- [27] M. J. Ahmadi and T. M. Duman, "Random spreading for unsourced MAC with power diversity," *IEEE Commun. Letters*, vol. 25, no. 12, pp. 3995–3999, Oct. 2021.
- [28] K. Hsieh, C. Rush, and R. Venkataramanan, "Near-optimal coding for many-user multiple access channels," *IEEE J. Sel. Areas Inf. Theory*, vol. 3, no. 1, pp. 21–36, Mar. 2022.
- [29] H. Liu, Z. Bai, H. Lei, G. Pan, K. J. Kim, and T. Tsiftsis, "A new rate splitting strategy for uplink cr-noma systems," *IEEE Trans. Vehicular Tech.*, Apr. 2022.
- [30] M. Elhattab, M. A. Arfaoui, C. Assi, A. Ghayeb, and M. Qaraqe, "On optimizing the power allocation and the decoding order in uplink cooperative noma," *arXiv preprint arXiv:2203.13100*, Mar. 2022.
- [31] S. Sesia, "Techniques de codage avancées pour la communication sans fil, dans un système point à multipoint," Ph.D. dissertation, Télécom ParisTech, 2005.
- [32] W. Lee, O. Simeone, J. Kang, S. Rangan, and P. Popovski, "HARQ buffer management: An information-theoretic view," *IEEE Trans. Commun.*, vol. 63, no. 11, pp. 4539–4550, Aug. 2015.
- [33] W. Yafeng, Z. Lei, and Y. Dacheng, "Performance analysis of type III HARQ with turbo codes," in *Proc., IEEE Vehicular Tech. Conf.*, vol. 4, Apr. 2003, pp. 2740–2744.
- [34] D. N. Rowitch and L. B. Milstein, "On the performance of hybrid fec/arq systems using rate compatible punctured turbo (rcpt) codes," *IEEE Trans. Commun.*, vol. 48, no. 6, pp. 948–959, Jun. 2000.
- [35] P. Frenger, S. Parkvall, and E. Dahlman, "Performance comparison of HARQ with chase combining and incremental redundancy for HSDPA," in *Proc., IEEE Vehicular Tech. Conf.*, Oct. 2001.
- [36] M. Danieli, S. Forchhammer, J. D. Andersen, L. P. Christensen, and S. S. Christensen, "Maximum mutual information vector quantization of log-likelihood ratios for memory efficient HARQ implementations," in *Proc., Data Compression Conf.*, Mar. 2010.
- [37] W. H. Equitz and T. M. Cover, "Successive refinement of information," *IEEE Trans. Inf. Theory*, vol. 37, pp. 269–275, Mar. 1991.
- [38] V. Kostina and E. Tuncel, "Successive refinement of abstract sources," *IEEE Trans. Inf. Theory*, vol. 65, no. 10, pp. 6385–98, Jun. 2019.
- [39] J. Østergaard, U. Erez, and R. Zamir, "Incremental refinements and multiple descriptions with feedback," *IEEE Trans. Inf. Theory*, May 2022.
- [40] T. Helleseth, D. J. Katz, and C. Li, "The resolution of Niho's last conjecture concerning sequences, codes, and Boolean functions," *IEEE Trans. Inf. Theory*, vol. 67, no. 10, pp. 6952–62, Jul. 2021.
- [41] H. Liu, N. Polianskii, I. Vorobyev, and A. Wachter-Zeh, "Almost affinely disjoint subspaces," *Finite Fields and Their Applications*, vol. 75, p. 101879, Oct. 2021.
- [42] M. Shirvanimoghaddam, "On the Hamming weight distribution of subsequences of pseudorandom sequences," in *Proc., IEEE ISIT*, 2021, pp. 1671–1675.
- [43] H.-J. Zepernick and A. Finger, *Pseudo random signal processing: theory and application*. John Wiley & Sons, Jul. 2013.
- [44] Q. Yu and K. Song, "Uniquely decodable multi-amplitude sequence for massive grant-free multiple-access adder channels," *arXiv preprint arXiv:2110.11827*, Oct. 2021.
- [45] R. W. Yeung, *Information Theory and Network Coding*. Springer Science & Business Media, 2008.
- [46] Y. Polyanskiy, H. V. Poor, and S. Verdú, "Channel coding rate in the finite blocklength regime," *IEEE Trans. Inf. Theory*, vol. 56, no. 5, pp. 2307–59, Apr. 2010.
- [47] D. Tse and P. Viswanath, *Fundamentals of Wireless Communication*. Cambridge University Press, 2005.
- [48] T. M. Cover and J. A. Thomas, *Elements of Information Theory*. John Wiley & Sons, 2012.